A Novel Approach To Accommodative Human Intraocular Lenses

BY

MATTIAS MENGONI
Laurea, Universitá Politecnica delle Marche, Ancona, Italy, 2011
Laurea Magistrale, Politecnico di Torino, Turin, Italy, 2014

THESIS

Submitted as partial fulfillment of the requirements
for the degree of Master of Science in Electrical and Computer Engineering
in the Graduate College of the
University of Illinois at Chicago, 2015

Chicago, Illinois

Defense Committee:

Prof. Vitali Metlushko, Chair and Advisor
Prof. Danilo Demarchi, Politecnico di Torino,
Prof. Danilo Erricolo
Prof. Bruce Gaynes, Loyola University Chicago
Prof. Anuradha Khanna, Loyola University Chicago

Dedicated to my dear father *Flaviano*

and to my dear mother *Ornella*, who would have loved to read this work.

1952 – 2008

ACKNOWLEDGMENTS

The desire that guides me in my endeavours

is the one to harness the forces of nature

to the service of mankind.

Nikola Tesla

This long but rewarding work, which I am hoping will continue and contribute to the wellness of mankind, has overlapped with what I like to call my first great adventure, which marks an important period in my life and personal growth, as well as the passing of my *shadow line*. I have had the fortune to share this moment with many great individuals, to which my gratitude is due for shaping this year as one I will forever treasure in my memory. First, I am sincerely grateful to my advisor Professor Danilo Demarchi, who has inspired me to pursue my interest in nano-scale systems and physics, and who has always been available for me whenever I needed, providing great advices and for encouraging me to broaden my horizons outside of my home country, as well as being a great mentor for just about anything. I would also like to express my great gratitude to my UIC advisor Professor Vitali Metlushko, to whom I owe many important teachings both in research and in life, having always provided great help and motivation to achieve great things. I can say without any doubt that I am proud to have been his student, and that I regard him as a great personality in my life. I am thankful also to my dear friend Federico, with whom I have shared most of my days in this past year. We have shared great

memories and difficult moments, but we made it through together, and I couldn't ask for a better companion in this adventure. We have both worked intensely on this project, and seeing it come finally to light is a great testament of what we managed to accomplish together. I wish you luck whatever you decide to make of your future, as we are now parting ways. I am very grateful also to Doctor Bruce Gaynes and Doctor Anuradha Khanna of Loyola University, who have provided exceptional insight and support and to whom I credit many of the design ideas I have come up with. To me you have been the guiding light in a field with whom I wasn't familiar before. I am thankful to my partners in this project: Debopam Datta, Khodr Maamari, Rohit Nathani. You have been all the most exceptional companions and we have shared and accomplished a lot together. I can claim with pride to have been part of one great team, and I hope our paths to cross again in the future. I would also like to express my most sincere and profound gratitude to my father Flaviano and my mother Ornella, without whom I wouldn't have been able to achieve as much in life. I owe them an unflinching and continuous support all throughout this path, and precious life teachings that have shaped into what I am today. Thank you, from the bottom of my heart, for everything. A special mention goes also to my sister, her husband Diego and to my nephew Lara, for providing me solace and moments of relax in between my commitments. You are a great family to have, and other than thanking you dearly, I wish you all the best in the future to come. A word of gratitude goes also to my other companions in this great adventure, the "TOP" guys: Alessandro, Andrea, Cesare, Daniele, Davide, Emmanuel, Giorgio, Valentino. I wish I had knew you all sooner, for we have shared some of the greatest moments of this journey. I couldn't ask for better companions.

ACKNOWLEDGMENTS (Continued)

A mention goes also to all the great friends I have made during this year in Chicago, both American and European: you are far too many to list, but I have been very lucky to know you all and to share time together. Last but not least, thanks to Anna Chiara, the woman who had to endure our distance in such a challenging year for her, and whose support has always been there for me, as if we were together through it all. And finally, a word for Chicago, "the city of big shoulders": I couldn't have asked for a better place to be. You are my "home away from home", and I haven't given up on you yet.

MM

TABLE OF CONTENTS

TABLE OF CONTENTS (Continued)

CHAPTER **PAGE**

LIST OF TABLES

LIST OF FIGURES

LIST OF FIGURES (Continued)

LIST OF ABBREVIATIONS

AC	Anterior Chamber (of the eye)
AC	Anterior Chamber Lens
DALY	Disability-adjusted life year
AFM	Atomic Force Microscopy
CMTF	Critical Modulation Transfer Function
CNT	Carbon Nanotube
CVD	Chemical Vapor Deposition
DUV	Deep Ultra-Violet
EBL	Electron Beam Lithography
ECCE	Extra-Capsular Cataract Extraction
FE	Field Emission
HSQ	Hydrogen Silsequioxane
IAPB	International Agency for the Prevention of Blindness
ICCE	Intra-Capsular Cataract Extraction
IOL	Intra-ocular Lens
MBE	Molecular Beam Epitaxy

LIST OF ABBREVIATIONS (Continued)

MEMS	Micro-electro-mechanical system
MAP	Multi-photon Absorption Polymerization
MRI	Magnetic Resonance Imaging
NCF	Nanotechnology Core Facility
Nd:YAG	neodymium:yttrium-aluminum-garnet
OPC	Optical Proximity Correction
SAD	Self-amplified de-polymerization
SPL	Scanning Probe Lithography
PC	Posterior Chamber (of the eye)
PCO	Posterior Capsule Opacification
PE	Phacoemulsification
PGMEA	Propylene Glycol Methyl Ether Acetate
PL	Photolithography
PR	Photoresist
PMMA	Poly(Methyl MethAcrylate)
RIE	Reactive Ion Etching
RCS	Refractive Cataract Surgery
SEM	Scanning Electron Microscopy

LIST OF ABBREVIATIONS (Continued)

SIA	Surgically-Induced Astigmatism
TFE	Thermal Field Emission
UIC	University of Illinois at Chicago
VA	Visual Acuity
WHO	World Health Organization
XUV	Extreme Ultra-Violet

SUMMARY

This thesis work presents a novel design of a passive ultra-thin *IOL*, which is the only effective method for treatment of cataract, a condition responsible for the majority of the world's blindness cases. The lens is designed in a Fresnel shape, which is set to minimize surgical impact and to restore full-range vision without any need for an external power supply. This *IOL* presents potential to be more a more reliable, versatile, cost and time effective alternative than the current state of the art iterations.

The first part of this work focuses on discussing the statistics on cataract surgery, the current state of the art *IOLs* and the theoretical background on human and rabbit eye anatomy, as well as an overview of regulations on laboratory testing. The design will focus on the rabbit lens, as it is a crucial experimental step since tests on humans cannot be directly carried out, even if they are the final user of the *IOL*. The second part focuses on discussing the idea and design of the lens, presenting both the standard approach and some alternative solutions, including the one here presented, with a discussion on trade-offs. The third part focuses on discussing fabrication of the *IOL* mold by means of advanced 3D electron beam mix and match lithography, and characterization of the final sample. Comparisons with *IOLs* currently available on the market are also presented. Using all acquired data it will then be possible to try several similar accommodative designs, as well as designing haptics for full force transfer from the ciliary muscles to the *IOL*. All these and future developments are discussed in the conclusion.

CHAPTER 1

INTRODUCTION

1.1 The blindness problem

Eye blindness and visual impairment have constituted a major problem for the human race since its dawn, which despite the advancements in both the understanding of human anatomy and physiology, as well as technologies for correction and therapy, is still largely impacting humanity nowadays.

Specifically, about 45 million individuals are completely blind while 135 million are visually impaired, accounting roughly for 4% of the total world population. Not only that, but an estimated 3.1% of the total world's deaths are directly or indirectly linked to cataract, glaucoma[1], trachoma[2], and onchocerciasis[3]. In addition, it is worth noting how about 80% of the visually impaired population is chiefly located in rural areas of less developed nations, especially in Africa and Asia, with respectively 7 million and 27 million concentrated in sub-saharan Africa, making up 0.3% to 1.3% of the total world population in blindness[4] and 1.4% to 3.6%

---

[1]A group of eye conditions that lead to damage of the optic nerve, responsible for the transmission of visual information from the eye to the brain.

[2]A bacterial infection of the eye.

[3]A Neglected Tropical Disease (NTD), also commonly referred as "river blindness", which develops through the parasitic presence of a worm, namely the Onchocerca volvulus.

[4]According to the WHO, blindness is considered to be a VA inferior than 20/400 (feet) or 3/60 (m).

in lowered visual acuity (VA). These figures, as estimated by the World Health Organization (WHO), establish Africa as the most affected region, even though this does not mean other world nations are faring any better: Myanmar for instance boasts one of the highest blindness rates at national level, while in the Americas and Caribbean region Haiti shows ten times the incidence rate of such illnesses compared to Canada.

Given the wide diffusion of blindness and visual impairment in less developed nations, which notoriously have reduced access to modern and expensive treatment solutions compared to first world countries, and the overall high incidence in the world nevertheless, many eye health initiatives around the globe have been launched in the last decades to address these issues, of which the most important is VISION 2020: The Right to Sight. Sponsored by the WHO in partnership with the International Agency for the Prevention of Blindness (IAPB), its objective is to extinguish avoidable blindness by 2020.

In this regard, the cataract, which encases the crystalline lens of the eye in all living beings, is currently the leading reason of blindness world-wide, estimated to be responsible for 48% of the cases . As such, treating cataract defects is a major step towards reaching the goal of VISION 2020. Cataracts affect approximately 18 million people, 90% of whom are in low to middle income countries, with the rates of blindness or low VA being much higher in specific countries as evidenced previously. In the Kilimanjaro Region of Tanzania for example, cataract alone accounts for 52.4% of blindness and 70.6% of visual impairment. In the Americas, Chile and Brazil display rates of incidence of 55 and 62%, respectively, and among the Caribbean

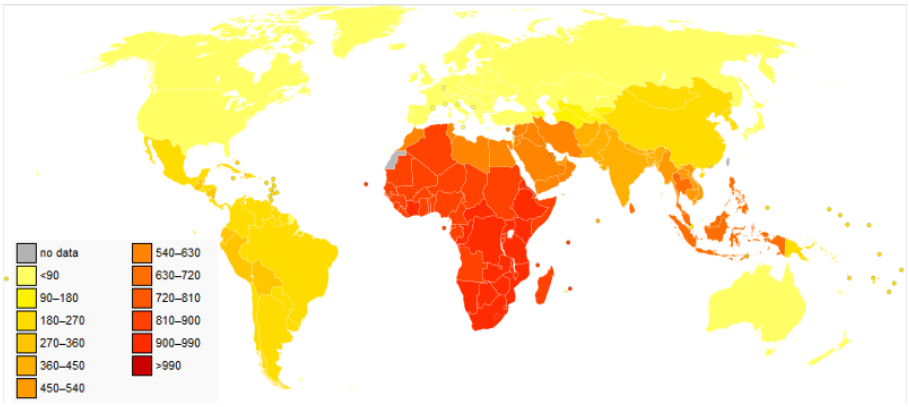

Figure 1: Disability-adjusted life year (DALY) rates due to cataract by country, standardized by age (every 100.000 individuals).

nations cataract is responsible at 60%. Locally in Chimbote (Peru) and Campinas (Brazil), the rates reach percentages as high as an estimated of 72 to 74%. Figure figure 1 shows the effect of cataract world-wide.

In regards to the United States, cataract remains the leading cause of vision loss despite having one of the lowest rates of all countries. It was also statistically proven how cataract-induced blindness is especially high in the Hispanic and African-American populations at 27%. Cataract-related interventions encompass roughly 60% of all Medicare costs related to vision. It can be also easily predicted how cataract problems will increase as the population ages and risk factors become more prevalent in time, such as diabetes. [6] According to some projections [9], cataract-affected population in the United States will increase by 50 and rise to 30.1 million by 2020.

It is worth focusing the study also on the younger portion of the population. Cataract can be present at birth due to various reasons, such as prenatal infections (rubella, cytomegalovirus), maternal diabetes and hereditary disorders, which are referred to as congenital cataracts. Those are particularly severe, so to guarantee good vision and sensory functionality for the child, timely surgical intervention is extremely important. Not only that but visual deprivation during the pre-cortical stage of visual development, which is the first 6 weeks of life, will result in lazy eye (amblyopia[1]) and disturb development of binocularity. If cataracts are not removed within the first year of life, vision will never be fully regained. Furthermore, even though cataracts can be easily removed by surgery, it is imperative that the child receive glasses to correct loss of focus by removal of the lens; otherwise, the child will develop permanent visual impairment. as about 20% pediatric blindness can be attributed to cataract alone. In the Americas and the Caribbean, childhood blindness (defined as subjects under the age of 15) was estimated to account 0.45 out of 1,000 individuals, and even as high as 1.45 cases out of 1,000 for children coming from low-income countries in Africa and Asia.

This is acutely problematic for the poorest regions of Africa and Asia, as approximately three-quarters of the world's blind children are located in those two continents. Congenital cataract also affects the immediate family as it demands additional time to care for and assist the affected child, which can result in a disruptive financial burden in lower-income countries. Therefore, not only is blindness one product of poverty, but blindness can indeed further con-

---

[1]The loss of one eye's ability to discern details.

tribute to impoverishment. On the contrary, it is clear how a successful cataract surgery can instead improve a household's economic status, also given the estimation that better eyesight would enable more formal education. Thanks to improvements in surgical techniques that make it an outpatient procedure, cataract surgery is one of the most cost-effective of all health interventions. Even though that holds true, lack of insurance , and therefore cost, was the highest reason recorded [5] for being unable to have the procedure performed. Unlike in wealthier countries, such as Japan, where routine cataract surgery is highly cost-effective for both eyes , cataract extraction can be performed, for example, in Myanmar for $ 20, which is approximately 3 weeks of income for a village farmer.

Although it is difficult to measure exactly the total impact of blindness in society, the rates are nevertheless shocking and cannot be ignored. Low-income countries show higher rates of blindness, with a large percentage of the cases being caused by cataracts. Unilateral or bilateral cataract is a leading cause of treatable blindness. Although there are many drugs claiming to have anti-cataract properties around the world, there has been no evidence of effectiveness shown through rigorous clinical investigations. So far, the only truly effective treatment of cataract is surgery to replace the lens with an artificial implant, known as an intra-ocular lens (IOL).

1.2 Human Eye Anatomy

Before delving further in the discussion on IOLs and the surgical procedure for their implantation, it is crucial to understand how the human eye actually works and its structure.

The human eye is a conscious sense organ which allows light recognition and vision, including colour differentiation and the perception of depth, through the *rod* and *cone* cells in the retina. For simplicity purposes, the eye can be seen as a complex optical system which collects light from the surrounding environment, regulating its intensity (and thus also focusing on certain objects) and converting it into a set of electrical signals that will then be processed by the human brain into images.

In Figure figure 2 we may see a the layout of the human eye which is divided into two segments: anterior and posterior, with the former sub-divided into two chambers: Anterior (front - AC) and Posterior (rear - PC), separated by the *iris*. The anterior chamber, located between the *cornea* and the iris, contains aqueous humour, a fluid that provides nutrients to areas lacking blood vessels, which is the specific case for the *crystalline lens* and the cornea.

Light enters first into the cornea, a "window-like" transparent dome in front of the eye and part of the sclerotic coat, which is not transparent and contributes to the "white" of the eye. Its surface is kept moist and dust-free by secretions from the tear glands. The cornea accounts for about two-thirds of the optical power of the eye alone, being the area of strongest focusing power in the entire organ. It basically acts as a lens with a fixed focus. The cornea is made up of five layers, which are thinner towards the centre and with the outermost being the epithelium, which makes up 90% of it. As for humans, the diameter of the cornea is of about 11.5 mm with an overall central thickness between 0.5 and 0.6 mm, while at the periphery it spans between 0.6 and 0.8. The cornea is undoubtedly an important tissue of relevant complexity, due to

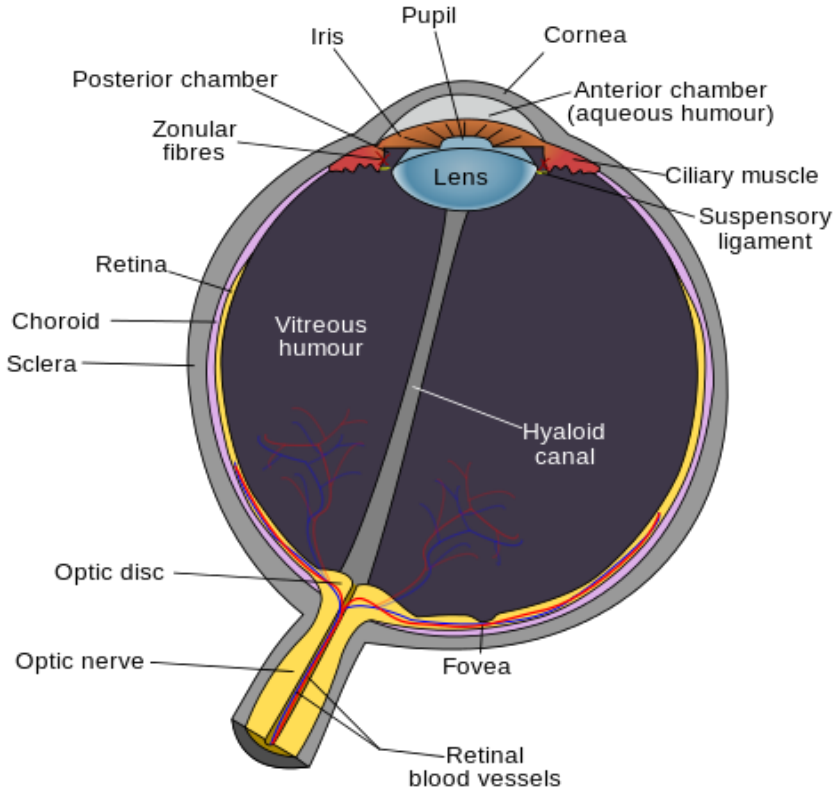

Figure 2: Schematic diagram of the human eye.

its properties of avascularity and transparency combined with immunologic privilege and the localization of resident immune cells, even if they are immature.

The amount of light entering the eye is then controlled by the iris, which expands and contracts in order to adjust the size of the pupil, which is the opening in the middle. The iris is made up of two layers: the *stroma*, a pigmented fibrovascular tissue at the front, and right

below it, pigmented epithelial cells, which are the most relevant factor to the characteristic iris colour and pattern, different for every subject.

The crystalline lens, which is the main focus in IOL surgery, will be dealt with in the following section in more detail.

Finally, the posterior segment of the eye comprises three distinct elements:

- The *vitreous*, which fills the eye with a jelly-like fluid, the *vitreous body*
- The *choroid*, containing blood vessels for the retina, which is responsible for reducing reflection-induced noise of stray light within the eye, improving the image-forming capabilities of the eye. Part of it forms the iris at the front, and it also contributes to the colour of the eye as it is pigmented
- The *retina*, which converts light into neurotransmitters by means of photo-receptors as underlying (below the interneurons' layer) rods and cones, each of the latter "tuned" to respond best to light from a portion of the spectrum of visible light.

1.3 Crystalline Lens and Accommodation

Loosely opposed to the iris in the posterior chamber, we find the crystalline lens of the eye, which is suspended at the equator by means of fibers called *zonules* that are attached to *ciliary muscles*. The physiology of the eye, or the active transport mechanisms of metabolites, is not of concern in this thesis. Rather, it is more important to understand the structure of the lens and its physical nature. Unlike the cornea, the lens' focus can be adjusted, which provides the remaining one-third of the eye's total optical power. The ciliary muscles along with the zonular

fibers enable changes in the lens shape by means of exerted force, which deform the lens back thanks to the capsule distributing such forces. It is worth noting how this is only a recent discovery [15], as for more than a century, it was assumed that focus changes in the lens were due to the relaxation of the lens zonules and the elasticity of the capsule only.

When the ciliary muscles are relaxed, the zonular fibers become taut causing the lens to flatten out and thus increasing long range focus. Contraction of the ciliary muscles pulls towards the axis of the eye making the lens more spherical and increasing the power for short range focus. In addition, the eyes converge and the pupil gets smaller. This entire process, called *accommodation*, focuses light onto the retina as shown in Figure figure 3. Accommodation and convergence both play a crucial role in depth perception as the brain estimates an object's distance by the amount of focusing involved.

In regards to the lens' physical structure, it can be regarded as a biconvex lens with different radii of curvatures, or as an asymmetrical oblate spheroid. Its thickness measures about 3.5 to 4.0 mm anterior to posterior (A-P) and diameter is typically between 9.0 to 10.0 mm. The overall structure of the lens is composed of three main parts: capsule, epithelium and fibers. The fibers form the interior of the lens and are then covered by the epithelium and encased by the lens capsule.

To further understand the lens' structure, the most employed techniques by the scientific community have been Atomic Force Microscopy (AFM) and Scanning Electron Microscopy (SEM), or Magnetic Resonance Imaging (MRI). This because there are no in-vivo measurement

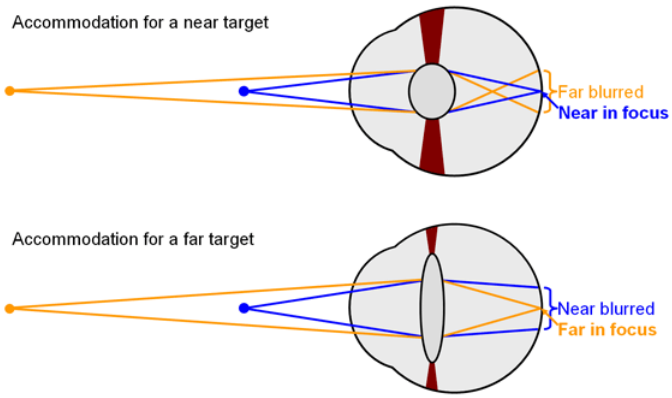

(a) Accomodation

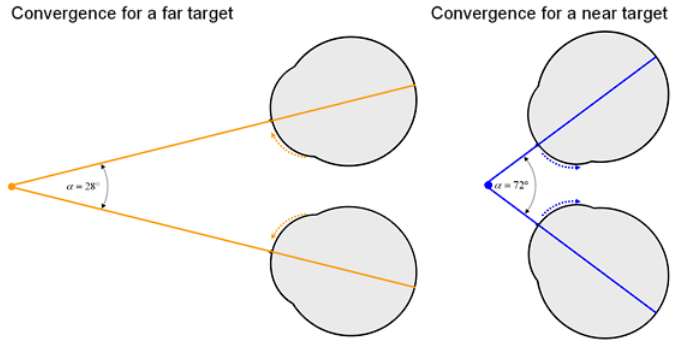

(b) Convergence

Figure 3: Accomodation and Convergence processes of the human eye.

solutions that have proven to be more reliable (even if they would be arguably more precise), while up until recently the only way was post-mortem measuring. These types of measurement technology not only allows scientists to see the lens in more detail but also enable more accurate measurement of the structures. The morphologic study of the lens' fibers by means of Scanning Electron Microscopy (SEM) has proven that the cells in embryonic and fetal nucleuses were of a rounded shape, while in the adult nucleus, they were flattened.

1.3.1 Lens defects and effects of aging

The human lens is not perfect and can have many refractive errors such as astigmatism[1], myopia[2], hyperopia[3], and presbyopia[4].

At birth, the lens' diameter approximately measures 6 mm. From then to the onset of boyhood the juvenile nucleus is formed by fibers of the lens gradually encasing the fetal nucleus. Eventually, the adult nucleus comes to formation by steady expansion of the fibers in the same fashion. The cortex on the other hand is made up by the peripheral fibers located between the capsule and the core. While the lens keeps maturing, the variation in the protein content of the lens will result in a gradient of the refraction occurring from the core of the structure. During the ageing process, specifically between the twenties and eighties, it has been found how the subjects' anterior lens surface radius exhibits a sharp decline, namely from 15 down to 8.5 mm, circa [1]. As for the posterior lens, its radius instead has a more contained decrease, accounting from 8.5 to circa 7 mm. As a result of this, noting how the other eye's dimensions

---

[1]An aberration due to the inability of the eye to focus to a sharp point on the retina, therefore making the image blurry.

[2]An aberration commonly referred to as near-sightedness, occurs when the lens cannot adjust to objects in the distance.

[3]An aberration commonly referred to as far-sightedness, it is the opposite of myopia and as such it's the inability of the lens to adjust to objects up close.

[4]An aberration consisting of the combination of myopia and hyperopia, which usually starts affecting people around the age of 45.

do not have as much of a significant alteration when growing older, we could postulate how in a later age there is a trend leading to myopia with an increased power of the lens. On the contrary, an hypermetropic shift is found to take place between the thirties and the sixty years of age. This feature has been named the "lens paradox", for which we have a reduced crystalline lens' radius of curvature of the lens with the age, in spite of the eye not turning increasingly myopic. In the end this process results in part of the loss of accommodation that comes with age. The rest can be attributed to elasticity. The lens retains all of the cells that it has formed since embryogenesis[1]. As the nucleus compresses during growth, it becomes less pliable. The nucleus also increases rigidity, a condition known as *sclerosis*, due to the incorporation of cholesterol with phospholipids in the membranes of the lens. The rigidity of the capsule, which is measured by the cholesterol-to-phospholipid ratio, also grows in the ageing process, thus leading to presbyopia with a subsequent loss of accommodation.

1.3.2 Cataract

As we have discussed before, since the primary function of the crystalline lens is to dynamically focus light entering through the iris onto the retina, transparency is fundamental. Such property is due to extraordinarily regular fiber arrangement and cell shape, regular cell volume, minimal extracellular space and minimal scatter elements. On top of this, a minimal spatial change in the refraction index related to the incident light's wavelength can be observed.

---

[1]The formation and development of the embryo, in which lens cells form very early.

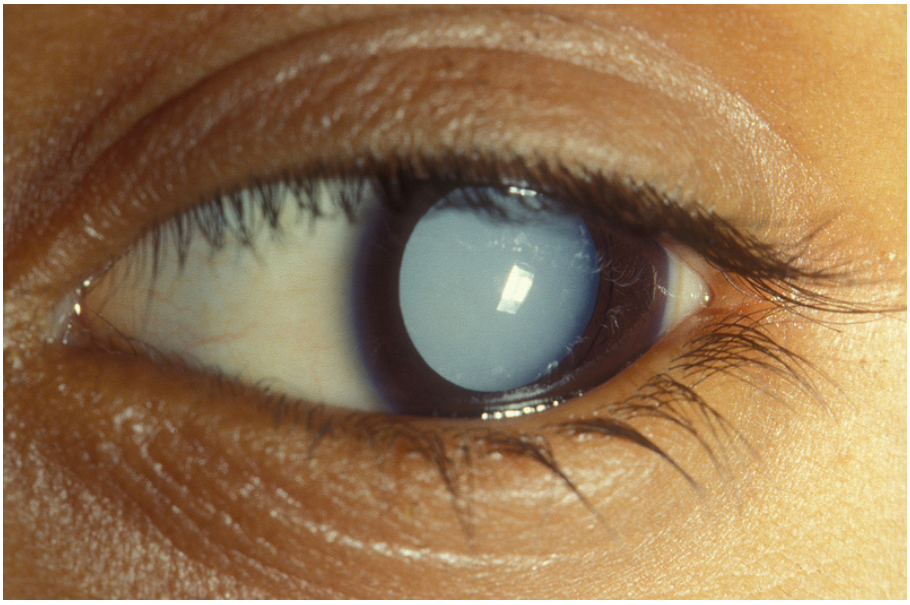

Figure 4: A mature cortico-nuclear cataract with white nucleus in a child.

Preservation of this unique structure allows the lens to maintain its transparency through all its development.

A cataract is a clouding of the lens, as in Figure figure 4, which lessens the VA and also results in aberrations such as monocular double or triple vision. There are many causes to the formation of cataracts: radiation exposure, long-term exposure to ultraviolet light, diseases (diabetes, for example), trauma and the natural aging process. Nuclear sclerosis, mentioned before for negatively affecting accommodation, deforms the cells, increases scattering and contributes to the formation of cataract. The natural suture planes also detract from the lens' optical quality.

Even though the lens is regarded to be mostly clear, there is a change in colour over the years, called *brunescence*, for which the fetal lens actually is a faint yellow colour, and an older lens may appear of a darker yellow, reddish brown, brown orange or even black. This effect is due to an age-related accumulation of *chromophores*, such as oxidized tryptophan (N-formylkynurenine) non-enzymatically glycated protein. Some amount of brunescence is beneficial because it reduces glare. However, advanced cases instead cause reduction in high-contrast acuity and sensitivity. There is good clinical correlation between light scattering, the intensity of brunescence and the hardness of the posterior nucleus, and this may contribute to cataract.

Transparency in the nucleus can also be lost through opacization when light-scattering foci in the nuclear fiber cytoplasm or nuclear plasma membrane are formed. These foci contain either huge protein aggregates from sulfhydryl (-SH) aggregates, which are oxidized to constitute protein-protein disulfide (-SS-) bonds or by larger molecules having higher indexes of refraction. Elevated concentrations of oxidant hydrogen peroxide (H2O2), which allow oxidation of nuclear components, were found in patients with maturity-onset cataracts.

1.4 Standard approaches to cataract surgery

In this section we will move onto cataract treatment, highlighting its history and different approaches with their pros and cons, especially in regards to IOL surgery. Removal of visually significant cataracts reduces the risk of injury to and improves the quality of life for a patient. Cataract extraction surgery has proven to be generally safe and highly successful. The modern combination of cataract removal and refractive surgery has created an ophthalmologic sub-

speciality of technology and surgeons: *Refractive Cataract Surgery* (RCS). RCS encompasses not only IOLs but breakthrough surgical technology as well.

Between 1960 and 1970, *Intra-Capsular Cataract Extraction*[1] (ICCE) became the method of choice because*Extra-Capsular Cataract Extraction*[2] (ECCE) had major complications. However, ICCE has its own complications too, like leaving the eye without any protective barrier between the AC and PC and, as a result, disturbance and stress affected the iris, vitreous, retina, and choroid. The ECCE method regained popularity due to *Phacoemulsification* (PE), which was invented in 1969 by Dr. Charles D. Kelman. The PE procedure involves lens emulsification through an ultrasonic handpiece and aspiration of the lens residual fragments. The removed fluids are then exchanged with a balanced salt solution, which is irrigated in order to preserve the AC, in addition to the benefit of cooling down the surgery toolpiece. As a result, ECCE may be performed through a small incision, which establish PE as a relatively safe procedure due to the equipment involved. Along with a foldable IOL implanted into the eye, PE provides less corneal distortion, less postoperative inflammation, lower *Surgically-Induced Astigmatism*[3] (SIA), and therefore also speeds up recovery time for patients. A visual example

---

[1]Removal of the lens and capsule in one piece.

[2]Removal of the lens while leaving the back of the capsule in place.

[3]Astigmatism is an increased difficulty to discern fine details, either close up or from a distance.

of PE and IOL surgery is shown in Figure figure 5. The severity degree of SIA varies according to the size of incision made and whether there are sutures and how many are used. Nowadays PE is the technique of choice in complete lens removal.

The actual surgery begins by putting the patient under general anaesthesia. Then, the eyelid is kept open by using a lid speculum, while the eyeball, or globe, is stabilized by a rod. A small, clear incision is made into the cornea, and viscoelastic gel is injected into the eye in order to stabilize the pressure and the internal structure. The cataract lens is then chopped into pieces and one-by-one brought into the anterior chamber, emulsified and then removed. Finally, once the nucleus and cortex are removed, a foldable IOL is implanted behind or in front of the iris. Because PE requires minimal incision, it allows for wound closure without additional sutures required.

It should also be noted however how complications may arise post-surgery in cataract treatment. *Posterior Capsule Opacization* (PCO), also known as *after-cataract*, is a clouding of the natural lens capsule following surgery, which may occur several months or even years after cataract surgery and may cause as much or more vision loss as the original cataract. There is a simple out-patient procedure carried out with *neodymium:yttrium-aluminium-garnet* (Nd:YAG) laser capsulotomy[1] that can correct this problem. Without the opaque capsule disrupting light, vision can then be restored.

---

[1]A laser incision into the capsule, such as in an operation to remove a cataract, carried out with a solid-state laser which uses as active laser medium an yttrium/ aluminium crystal neodymium-doped.

The discipline of RCS not only involves surgical methods and refractive IOL implantation, but also encompasses the refinement of post-surgery effects neutralization procedures. Thanks of the recent improvements in RCS, cataract-affected individuals are having surgery at earlier ages, and they are not only seeking correction of their disability, but also the improvement in post-surgery quality of life. The advancements in surgical methods are now considered to have reached their limits, with the future now seemingly lying only in even more sophisticated IOLs.

1.5 Intra-ocular lenses

1.5.1 History of IOLs

The first documented and widely accepted IOL implantation was performed on the 29th of November 1949 in London by Sir Harold Ridley, a demonstration of how this solution to cataract has been around for quite some time already. Ridley's IOL itself was a circular biconvex disc much like the shape of the natural lens with extensions from the optic component, known as haptics, to fix and stabilize it in the eye. The material employed in the making of the lens was a transparent thermoplastic: *Poly(Methyl MethAcrylate)* (PMMA), also known as acrylic glass, which was the same basic material used to manufacture cockpit canopies in airplanes of the period. A large part of this success is to be credited to the IOL manufacture by Rayner & Keeler, Ltd, UK, which is still today a prominent optical company in the United Kingdom. A testimony of this success can be found in how some of these original IOLs were functional in patients for over 40 years.

Despite their great innovation, there were some clear drawbacks to these early IOLs: AC collapse, glaucoma, uveitis[1], iris atrophy, and *capsular fibrosis*[2] due to the natural healing process. In addition to those conditions, the first generation lenses were much heavier due to the employment of PMMA and had poor fixation to the lens capsule, which allowed easier dislocation into the vitreous cavity.

In the 1950s, the second generation lens was developed: the *Anterior Chamber Lens* (ACL), which is shown in Figure figure 6. As it may be deduced by the name, this particular IOL was placed in the AC instead of the PC, where the first generation IOLs were implanted instead. This rendered the ACL procedure an easier one as the implantation was in front of the iris. Thanks to multiple haptics, angle fixation was enabled, with dislocation and loss into the vitreous cavity both prevented. Even so, there were still complications:

- The rigid haptic structure damaged the adjoining tissue
- The rotation of undersized IOLs or excessive vaulting caused contact to the cornea, or corneal endothelial, and led to opacization of the cornea, or *endothelial corneal dystrophy*
- An oversized IOL would cause chronic pain and inflammation to the patient

---

[1] An inflammation of the uvea.

[2] A clouding over the lens capsule membrane which holds the IOL in place.

- Impurity [BU] and initial poor quality finish of the PMMA in the early 1950s led to uveitis, glaucoma, and *hypema*, known as *UGH Syndrome*, which was still a problem well into the 1970s due to deformation of lens haptics.

In the late 1950s, a third generation lens was introduced: the *iris-supported* IOL, shown in Figure figure 7. These IOLs were still implanted in the AC but were instead affixed to the iris by means of sutures, metal clips, and haptics through the pupil. Their advantage compared to previous iterations was contact avoidance with the cornea and the chamber angle by being fixed to the iris. However, the procedure was now more complicated by the difficulty in lens placement, with dislocation problems still present. Other disadvantages included dehydration of the cornea, corneal decompensation, and adhesion between the iris and the vitreous, capable of causing papillary block.

Some of the complications with ACL were further addressed with the fourth generation IOLs:

- Increased flexibility of the haptics
- Irritation decreased by means of improved polish
- Sizing improved with multiple haptic diameters.

1.6 Rabbit Eye Anatomy

The idea of studying the rabbit eye anatomy is not a recent one, as the first dated attempt goes back to the 17th century, with the first reported experiment ran by the French Cocteau

and d'Etoille where they used the rabbit eye as a model for lens regeneration. This idea finds a justification in the fact that the rabbit ocular anatomy is akin to the human one, a reason for why even today it holds strong as one of the most frequently used non-human models in ophthalmic research, along with monkeys and cows.

In comparison to the overall dimensions of a whole rabbit, the eye is relatively big (in respect to the human ratio) and differs with ageing [2]. Once born the sphere is about 6 mm in diameter but it expands very quickly and at 7 to 10 days post-birth it is already about two-thirds the dimension of the adult ye. The antero-posterior dimension measures between 16 and 19 mm which makes it look like it is a bit compressed, the diameter at the equator is of approximately 18 mm. As we may deduct, the eye is of a more "rounded" shape compared to the bi-convex one with different radii of curvature of the human eye. As for the variation in focal power that can be achieved, the rabbit has similar accommodation means but with greatly reduced capability as compared to a human. The accommodative range of the rabbit's eye has been studied and it was concluded how it normally spans from 0 to approximately 2.5 diopters (D), even though in an adult speciment it is rarely above 1.5 D. In Figure figure 8 we may see a drawing of the actual rabbit lens structure.

This features, which makes the crystalline lens look more like a sphere, is actually of great help in designing. As we will see in the actual project in 2, it allows us to design a single sided lens capable of achieving the focal power of the double-sided lens very easily, thus making the final lens even thinner.

1.7 Motivation and Objective

The research described in this paper focuses on a future design of the IOL. The ultimate IOL should restore vision and accommodation entirely like the original lens of the eye. The ideas proposed in this paper build upon those of Nithya Jayapratha, whose work at the Nanotechnology Core Facility at the University of Illinois at Chicago (UIC) was the first to propose using micro-fabrication techniques in the creation of IOLs. In her thesis, a novel spiral design composed of micro channels that mimics the natural repeating patterns in the lens fibers was introduced. An optimal design was chosen by calculating the power of the lens taking into account the compression and elongation of the lens. Micro-fabrication techniques, such as deep ultra-violet (DUV) and X-ray lithography, were explored to fabricate better lenses that are also less expensive to fabricate. Finally, there was an investigation on various materials used in the process.

Jayaprathas research was not able to produce prototype IOLs with the required focal power for a fully accommodative eye. The micro-channels composing the IOL were too wide; especially compared to the fiber thickness of a natural lens. Ultimately, this was a limit imposed by the micro-fabrication technology used. However, the general concept of fabricating IOLs using micro-fabrication techniques remains to be novel, and the process shows great potential. This research further expands the fabrication of IOLs into the nano-manufacturing regime.

Nanotechnology will be used to fabricate molds of the spiral pattern, and soft lithography will be used to create the actual lens using flexible polymer materials. The flexibility is necessary for accommodation and should match that of the eye. By the end of this research, an

accommodative IOL will be fabricated using electron beam lithography in order to be implanted and tested in a rabbit model. Eventually, the lens could be implanted in infants and children following cataract surgery. The flexibility of the lens would compensate for some changes in growth of the eye during development thus providing clear vision without glasses at both near and distance for ones lifetime.

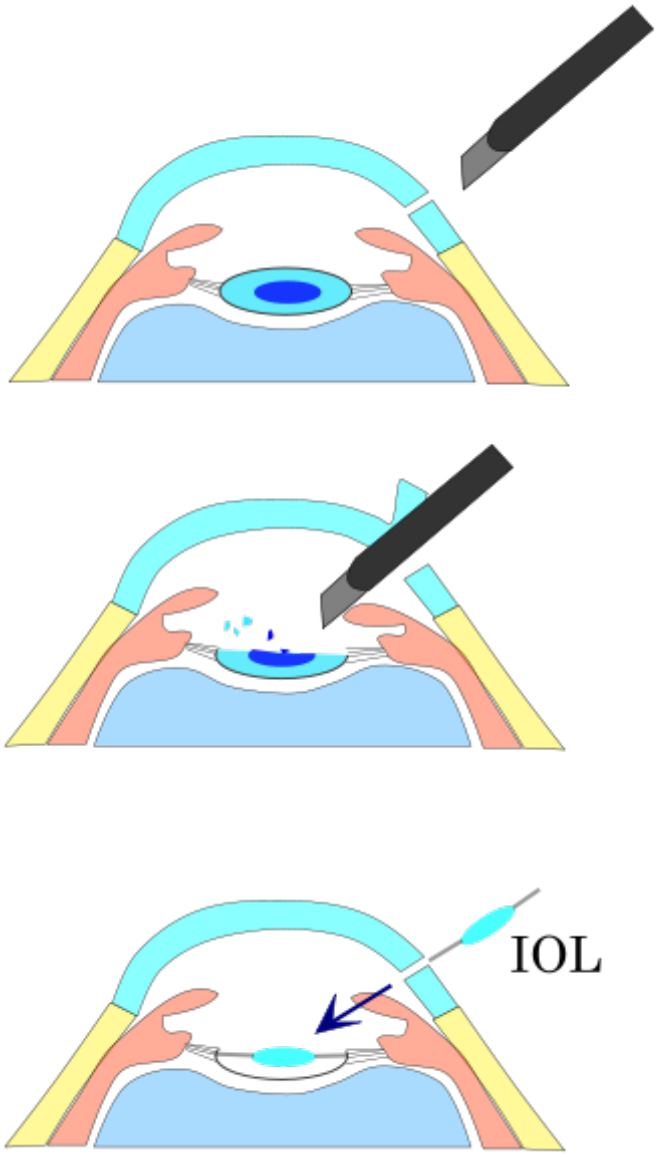

Figure 5: Phacoemulsification and replacement with Intra-Ocular Lens.

Figure 6: Anterior Chamber IOL.

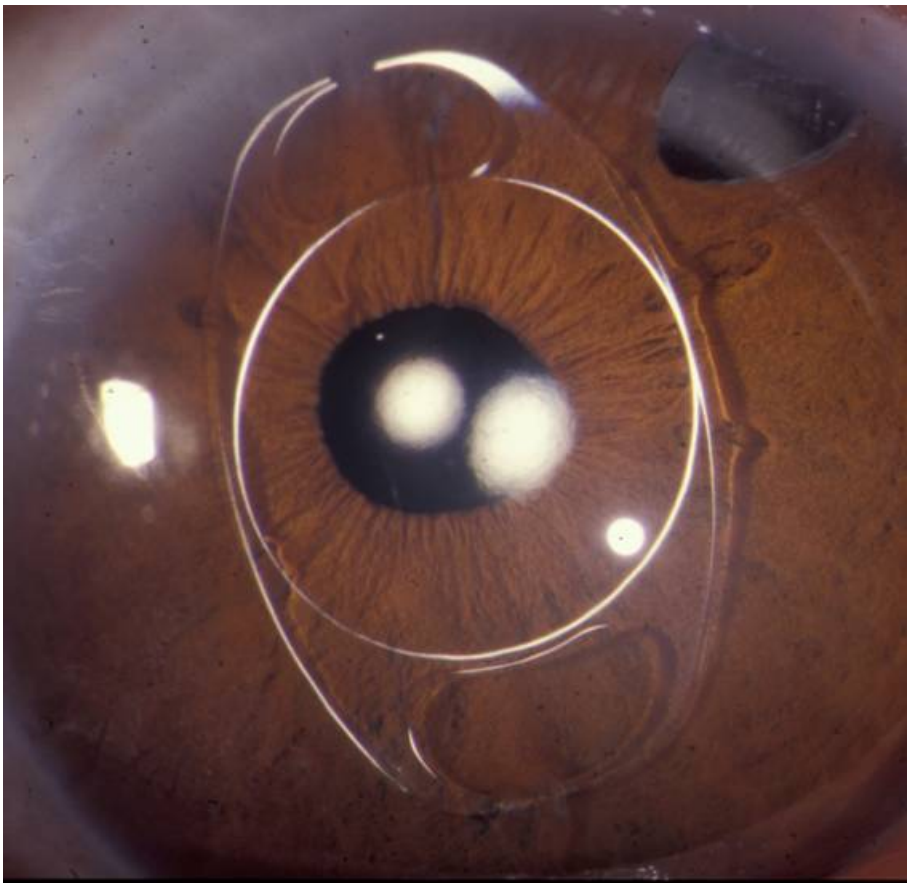

Figure 7: Iris-supported IOL.

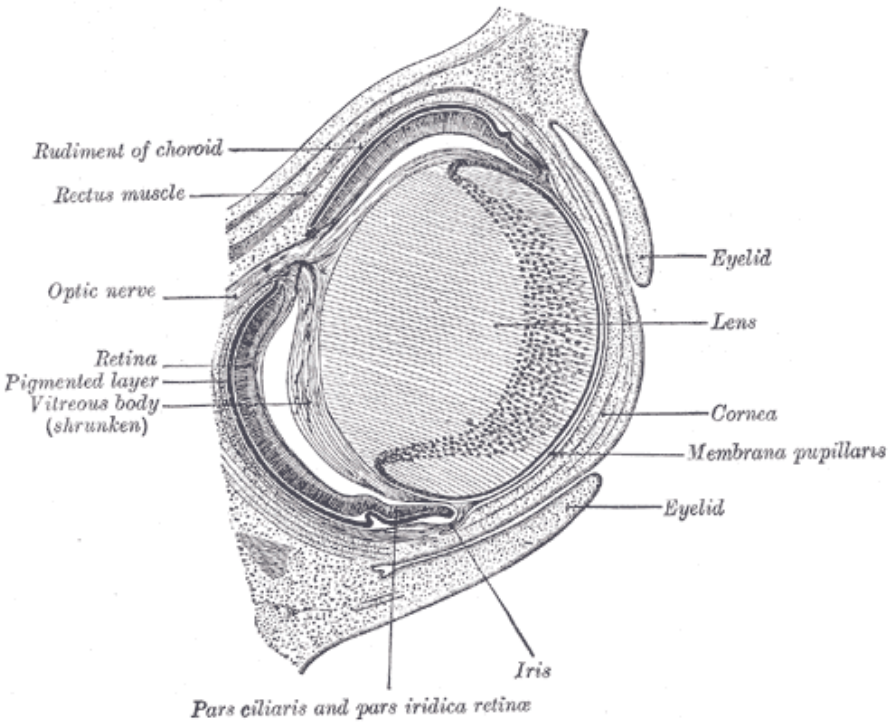

Figure 8: Cross-section of a rabbit eye.

CHAPTER 2

DESIGN

2.1 Eye equivalent model

The first thing we need to address in order to design an artificial crystalline lens for implantation, is to devise an engineering equivalent model to the biological one, on which we will then carry out design considerations. To this purpose, the basic element we will take into account is the lens, which is an optical device, typically made of any transparent material, through which the beam is converged or diverged, resulting in the transmission and refraction of light. A simple lens is made up by one optical element, whereas a compound lens can be seen as an array, arranged on a common axis, of simple optical elements (lenses). With the employment of several optical elements more aberrations can be corrected, compared to what could be achieved by a single element.

The eye of any mammalian in fact, be it rabbit in this specific case or human, can be modelled as an optical system made of several lenses placed at different distances. Such concept is highlighted in figure 9. The distance between the cornea and the retina is fixed and defined as the axial length t_{al}. Therefore, the focal power of the cornea is fixed. Spectacles or contact lenses, which may be worn by human individuals, are a located at a distance t_s from the cornea and are represented by the first lens from the left. Their focal power is specified by the prescription using the same properties of the lenses that we will shortly discuss. Lastly, the

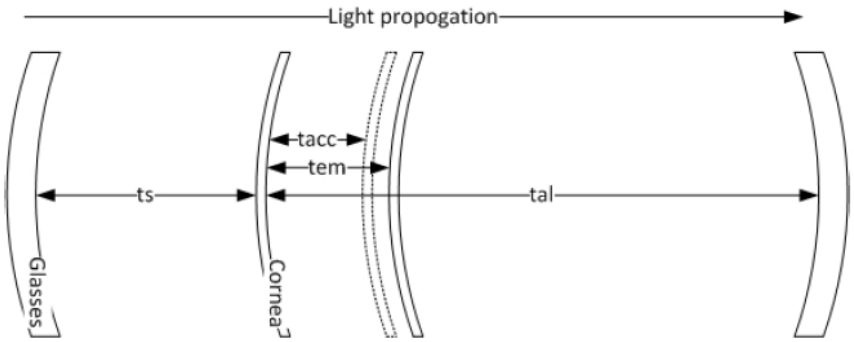

Figure 9: Equivalent optical system of the eye.

crystalline lens of the eye is responsible for the objects' final focusing, and is represented by the third solid lens. As explained in Section 1.3, the lens may change focal power as required by means of a change of shape in the lens. This same effect can be achieved alternatively by shifting the lens forward and backward, which is the actual process behind some IOLs, already highlighted in **??**. When the crystalline lens is in a relaxed state, or emmetropia, the distance from the cornea is designated t_{emm}, while when fully accommodated the lens is shifted forward as the dotted line lens in the figure, at a distance from the cornea defined as t_{acc}.

2.2 Basic optics

Having established an equivalent physical system, we now need to set some conventions in order to analyse and manipulate such system. In this chapter we will address fundamental optical principles on which all the aforementioned lenses are based. This will also enable us to

develop familiarity with some of the main terms and laws used in optics that will be further needed in order to measure and compare any type of lens.

The broad subject that is basic optics can be categorized into geometrical (or ray) optics, dominated by the physical phenomenon of refraction, and physical (or wave) optics, which is dominated by diffraction. The distinction lies on the physical dimensions of the objects involved in contrast to a given wavelength of the incident ray. Since we are dealing with mammalians such as humans and rabbits, we are working with visible light, usually defined has having a wavelenght in the range of 400 nm to 700 nm [3]. Given that the human and rabbit lenses have are of several orders of magnitude larger than visible light, we may only focus our study in the geometrical optics domain.

2.2.1 Refractive index

The *mean refractive index* n is a dimensionless figure [4] which describes the manner of propagating through a medium by a radiation (or more broadly, light), and it is established as:

$$n = \frac{c}{v_{phase}} \tag{2.1}$$

which is a ratio of c, which is the speed of light when the radiation is propagating through vacuum ($299792458\frac{m}{s}$) and phase velocity of light in the specific medium v_{phase}. Sometimes called the *mean refractive index*, it is measured in the middle of the visible spectrum (yellow-green colours). Specifically, the index can be measured at 587.56 nm wavelength for the helium "D" line (n_D) or 546.07 nm for the mercury "E" line (n_E). This because the refractive index of materials is not constant for all wavelengths of light.

Constringence (also called *Abbe number*) relates the mean refractive index of the blue and red ends of the visible spectrum, and it's an indication of the medium's dispersion (which is a change in the refractive index with the wavelength) in comparison to the refractive index. High constringence is indicative of the material having low dispersion, or few chromatic aberrations. Such value can be calculated as:

$$n = \frac{n_d - 1}{n_f - n_c} \tag{2.2}$$

where n_D, n_F and n_C are the refractive indexes of the material, in the case where wavelengths of the Fraunhofer "D", "F" and "C" spectral lines are employed (589.3 nm, 486.1 nm and 656.3 nm respectively). Constringence's reciprocal is dispersive power, which is actually more commonly employed for measurements.

The effect of constringence is most observable in how different colours of light are spread by a prism. If this occurred in an actual IOL, the colour fringing would be disruptive for vision quality. Therefore such measure has to be kept at a minimum in the materials used for IOL fabrication. Luckily, constringence tends to decrease as the refractive index increases. Poly(methyl metacrylate) (PMMA), one of the most common materials employed in IOL fabrication, has a measured value of 58, which is the same as the high-index crown glass used in the early production of glasses.

The refractive index gives an understanding of how much light is refracted when it travels through a medium, the actual motive behind the functionality of any lens. When a radiation penetrates the interface between two materials, and there is a gradient in the two refractive

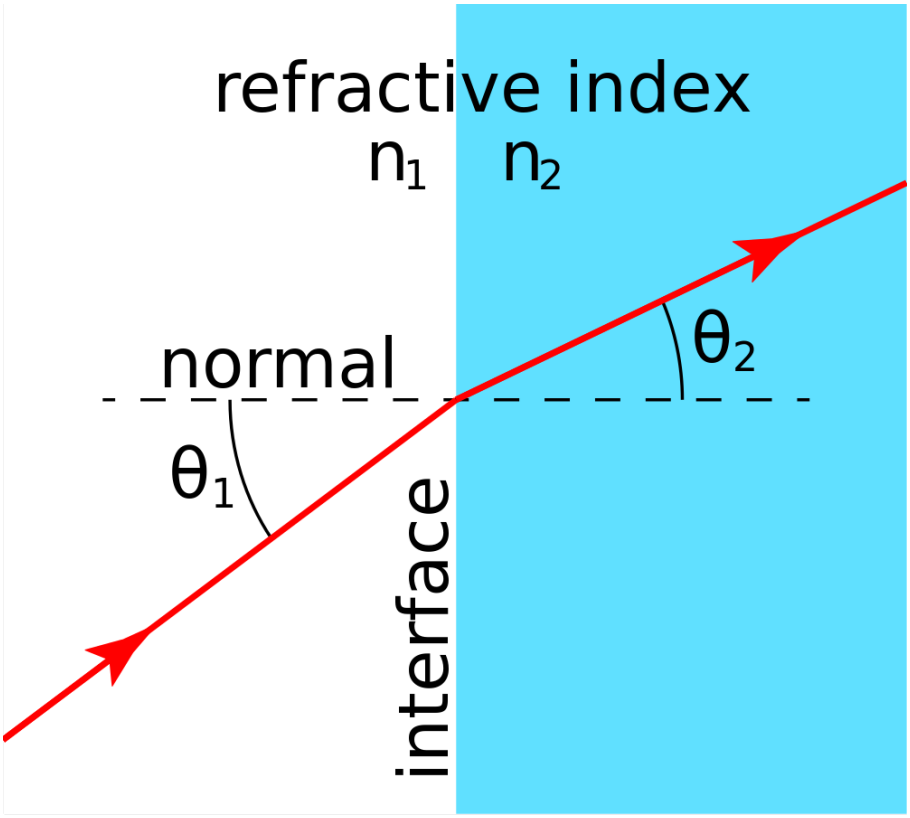

Figure 10: Refraction effect between two mediums with different refractive indexes.

indexes, the effect of refraction takes place. This causes a change in the speed of propagation, and thus a light ray incident on the interface, for every angle other than directly normal (90), will leave the interface at a different angle, as shown in figure 10.

$$n_1 sin\theta_1 = n_2 sin\theta_2 \tag{2.3}$$

This phenomena can be explained via Snell's law of refraction, Equation 2.3. There, θ_1 and θ_2 are the incident and refraction angles, respectively, of a light ray travelling through the interface between two materials, characterized by the refractive indices n_1 and n_2. The refractive indexes also establish the amount of light that gets bounced back (reflected) when it hits the interface, other than Brewster's angle, and the critical angle for which we have complete internal reflection.

As such, the refractive index can be regarded as an indication of how much the angle changes when crossing two different materials. The higher the refractive index, the more a lens bends light, and the thinner a lens can be. The change in angle along a non-planar surface, such as a sphere, results in a converging or diverging effect that causes magnification. Fundamentally, a lens is simply an object that converges or focuses light to a certain point, which in living subjects is the retina.

A simple and effective example of refraction can be found in how objects appear to be bent underwater. The interface is made up of water with $n = 1.333$ and air with n close to 1, with light rays bending when they exit (and enter) the water. The cornea and aqueous humour have a refractive index of 1.376 and 1.336, respectively, and are very close to that of water. The lens, however, has a higher index of refraction: 1.406. [28] Therefore, when we see under water, most of the light is bent only by the lens and not the cornea or aqueous humour.

2.2.2 Optical power and focal distance

The focusing capability of a lens system is expressed in terms of optical power and focal distance. The *focal length* of a lens is the distance (f) from a lens at which collimated rays

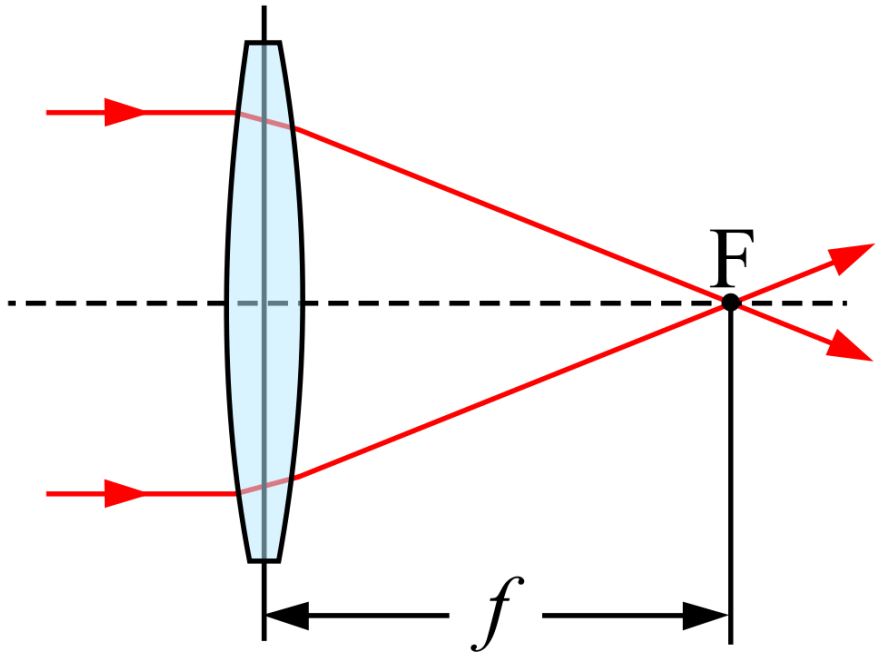

Figure 11: Convergence of light rays after passing through a lens.
Image released in the public domain.

converge, as shown in Figure figure 11. Focal length can be measured with any unit of length, yet it is usually given in meters (m) for theoretical calculations and millimeters (mm) for camera lenses used in photography.

If we assume the thin lens approximation, the formula in Equation 2.4 shows how focal length relates to the focusing of an image: specifically, the distance to an object S_o, and the distance to the image in focus, S_i:

$$\frac{1}{f} = \frac{1}{S_o} + \frac{1}{S_i} \tag{2.4}$$

At a very large range, as when looking at an object at the horizon, S_o approaches infinity. The equation then results in the image being in focus at the focal distance of the lens system:

$$\frac{1}{f} = \frac{1}{S_i} + \frac{1}{\text{inf}} = \frac{1}{S_i} \rightarrow f = S_i \tag{2.5}$$

Since images must be in focus on the retina and the eye size is fixed, the focal distance of the eye has to change in order to allow accommodation for objects at different ranges.

Optical power is also a measure of focus and is equal to the reciprocal of the focal length. The unit for power is dioptre (D), which is equal to an inverse meter (m^{-1}). Using the power (P) (or vergence), V_O and V_I of the object and image, respectively, simplifies the lens equation by removing the reciprocal terms and making them directly additive. This becomes especially useful in dual lens systems as it allows the lens' powers to easily sum.

$$P = V_O + V_I \tag{2.6}$$

For a thin lens the focal distance can be calculated with:

$$P = \frac{1}{f} = (\frac{n_2 - n_1}{n_1})[\frac{1}{R_1} - \frac{1}{R_2}] \tag{2.7}$$

where n_1 and n_2 are the refractive indexes of respectively the medium surrounding the lens and of the lens material, R_1 is the radius of curvature of the front of the lens and R_2 is radius of curvature for the back of the lens.

However, in practice, the thick lens equation is a better approximation for realistic lenses, as it takes into account the thickness between the front and back surfaces of the lens. The thick lens equation is also known as the *"lensmaker's equation"* and is represented as follows:

$$P = \frac{1}{f} = (\frac{n_2 - n_1}{n_1})[\frac{1}{R_1} - \frac{1}{R_2} + \frac{(n_2 - n_1)d}{n_2 R_1 R_2}] \tag{2.8}$$

where d represents the thickness of the lens. In general, an increased radius of curvature R will physically increase the thickness of the lens d, which is why higher refractive index materials will allow for higher power lenses without increasing their thickness. Another way to avoid a thicker lens while still achieving the desired power is to employ a Fresnel lens, which will be discussed in the next section.

2.3 Fresnel lens

A Fresnel lens, originally credited to Georges-Louis Leclerc, Comte de Buffon, is a thinner lens capable to achieve the same optical power of a normal biconvex lens but with a thinner design. An example of it, and the capability of collimating light rays, is shown in figure 12. The required amount of optical material is not as much as the one of a conventional lens, since by separating the lens into several concentric annular sections, it can still collimate light as a normal lens would. Compared to an equivalent simple lens, a Fresnel lens has an overall inferior thickness in every single secetion. The result of this is the division of the standard lens'

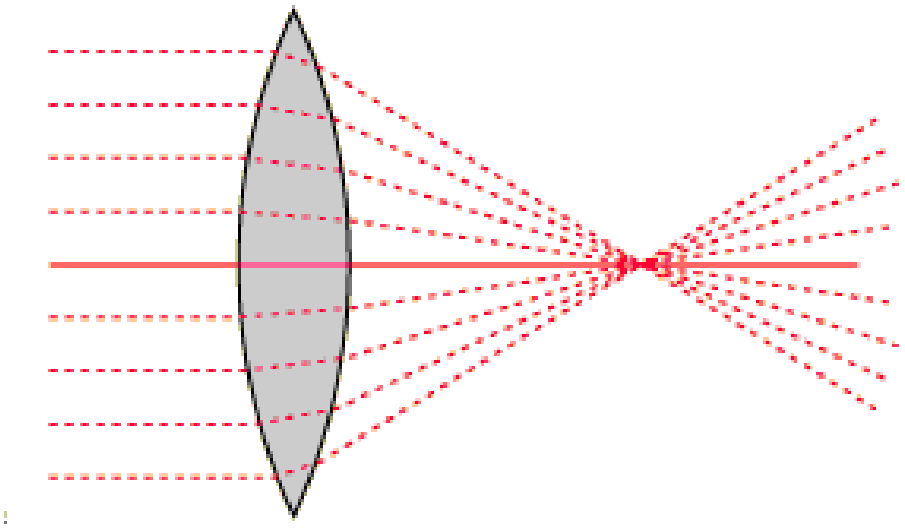

Figure 12: Convergence of light rays after passing through a lens.

continuous surface into a subset of surfaces all with equal curvature, with stepwise discontinuities between them. These obviously have the result of degrading image quality due to light scattering on those edges, resulting in diffraction and different travel times for the incident ray. Not only that, but different wavelengths of the visible spectrum will interact differently with those edges. This explains why in fields such as photography, conventional bulkier lenses are still preferred to preserve image quality. A comparison of a plano-convex lens and a Fresnel lens with the same optical power is provided in figure 13.

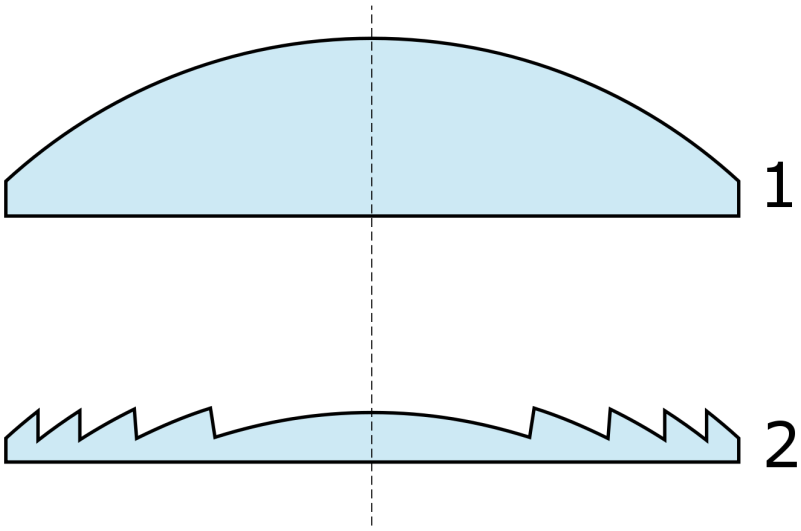

Figure 13: Plano-convex lens (1) and equivalent Fresnel lens (2).

Fresnel lenses have been employed throughout the last century mostly in lighthouses and spotlights, but they do enjoy a wide diffusion in most state of the art IOLs, as discussed in Chapter 1.7. Depending on the shape and direction of the lens in respect to the incident light, it can be act as a collector, collimator, or diverger, the first case being the one needed for an image to be focused as in our case. In this document I shall only focus on the conventional Fresnel lens design of the first order, but a much wider variety of shapes is available for different uses, all beyond the scope of this particular application.

2.4 IOL Project

2.4.1 Accommodation

Our main objective, as stated in section 1 is to have a fully accommodative IOL capable to focus on the whole visual range without the need of active force transfer from external source, but rather to employ a structure capable to flex with the force normally exerted by the ciliary muscles. One way to do this, as pointed out in 2.1 would be to shift the lens forward so that the focus point moves along the X axis in figure figure 9. The idea behind this work tries to exploit a simpler principle, which theoretically is easier to achieve. By removing lens material as to create cuts in the structure, we leave an hollow space like in Figure figure 14, which allows for the lens to be compressed and thus change shape as required for accommodation by the normal crystalline lens. This requires a flexible material, which will be discussed in **??** and a new concept of haptics which are not just used to keep the lens in place but rather to deliver the necessary force exerted by the ciliary muscles. The haptics will be further subject of research in the field, and is currently beyond the scope of this current work as a more rigid finite-element analysis must be carried out.

The cuts can be made of any possible shape, as in Figure figure 15, and it will be subject of future investigation to find the better haptic-cuts combination for full force delivery without the need to remove too much material while still maximizing accommodation capabilities.

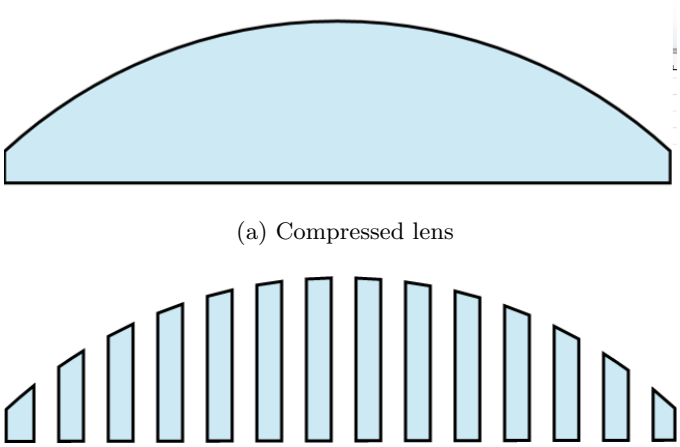

(a) Compressed lens

(b) Uncompressed lens

Figure 14: Side view of the lens with cuts.

For a Fresnel lens, as the case taken into analysis for this project, we may see an example of the structure with the cuts applied in figure 16.

For our project we have assumed the cuts to follow a spiral pattern starting from the centre of the lens, as it was already studied and demonstrated feasible in [5] and [6]. This work though does not focus on guaranteeing the necessary flexibility to the lens structure, which is addressed instead in [7]. The main contribution of this present work to the lens project, which is the actual Fresnel lens design, will be detailed in the next section.

(a) Compressed lens

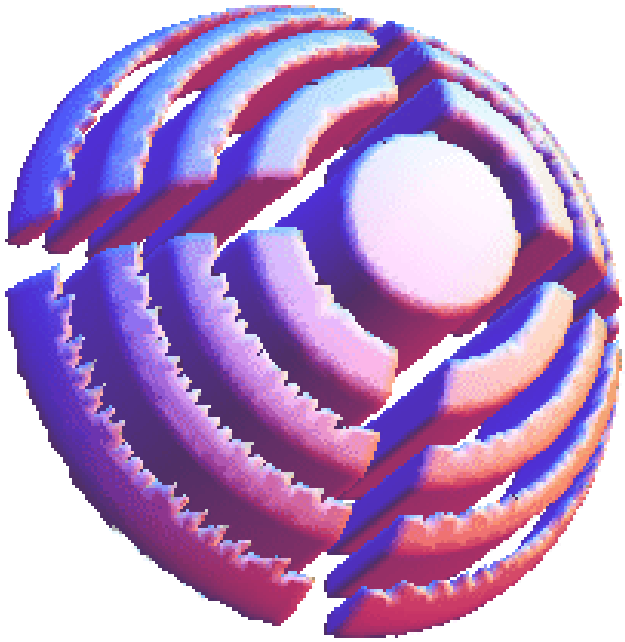

(b) Uncompressed lens

Figure 15: Top view of the lens with cuts.

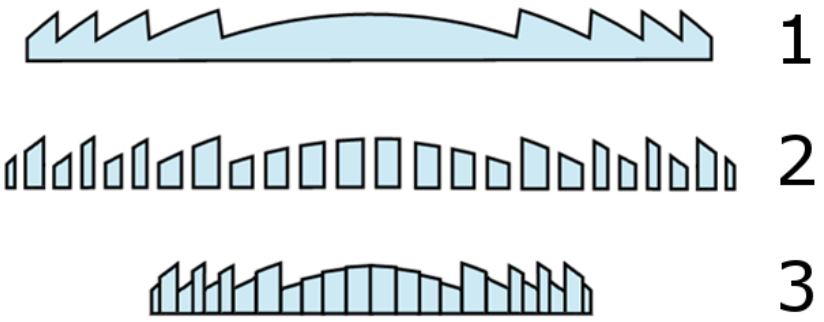

Figure 16: Side view of a Fresnel lens (1), an uncompressed equivalent with cuts (2), and a compressed equivalent with cuts (3).

CHAPTER 3

FABRICATION AND CHARACTERIZATION

3.1 Micro and Nano-fabrication

In this following chapter, we shall discuss the possible fabrication processes for our nano-scale Fresnel lens. This requires a totally different approach from the common lens-making which happens by milling a block of the selected transparent material in the desired shape, which in turn gives rise to several defects on the surface.

Micro-fabrication techniques emerged as the result of the increasing complexity and decreasing size of integrated circuits in very large scale integration (VLSI) technology. Although they are normally used in the manufacture of electronics, micro-fabrication processes and techniques have been adapted to mechanical systems since the 1970s [8]. In general, these devices are grouped into the category of micro-electro-mechanical systems (MEMS). Not only does micro-fabrication allow mechanical devices to be fabricated on the same chip as the electricity circuitry to which they are connected, but some devices, such as in micro-fluidics, might not have an electrical connection at all and rely on the mechanics of the device alone. Micro-fabrication has spurred several sub fields in different industries, of which BioMEMS is one of the most important, and under which this project falls under.

There are two different approaches to micro-fabrication: bottom-up and top-down. In the bottom-up approach, which is used less widely, the process starts with a blank substrate and the

structures are grown or assembled from original seeds. A substrate might start at the atomic or molecular level with a seed crystal or single polymer. This is referred to as self-assembly, which is found in the natural world. The bottom-up approach allows for smaller geometries than what is currently available using the top-down approach, but it is limited by the growth rates and therefore, working devices are difficult to mass produce. Currently, many labs are researching the creation of nanodots, nanowires, nanotube transistors, and monolayers using bottom-up approaches. Specific techniques that are commonly used in this approach are molecular beam epitaxy (MBE) and molecular self-assembly. The top-down approach represents the inverse idea and involves transforming bulk material into smaller devices. The first step is to create the bulk material that is going to be modified. Silicon wafers are common substrates and are cut from a large ingot grown from a single silicon crystal. Thin films are then deposited on the wafer through processes such as electron beam evaporation or chemical vapor deposition. The thin films are then shaped by either etching or lift off. Photolithography (PL) is the process by which patterns are created on the thin films. In PL a layer of photo resist (PR), which is a light-sensitive chemical, is spread on the wafer and/or thin film layer. The PR is then exposed to light and treated in a developer solution in order to reveal the pattern.

The PR can be either negative or positive. In positive PR, exposure to light breaks the bonds in the chemical and allows it to be removed in the developer. Negative PR performs in the opposite manner: exposure polymerizes the chemical, making it insolvent in the developer. The developer dissolves and removes the PR in the desired areas and a pattern is formed. The PR can protect portions of the metal from etching, or the PR can be dissolved to lift off the

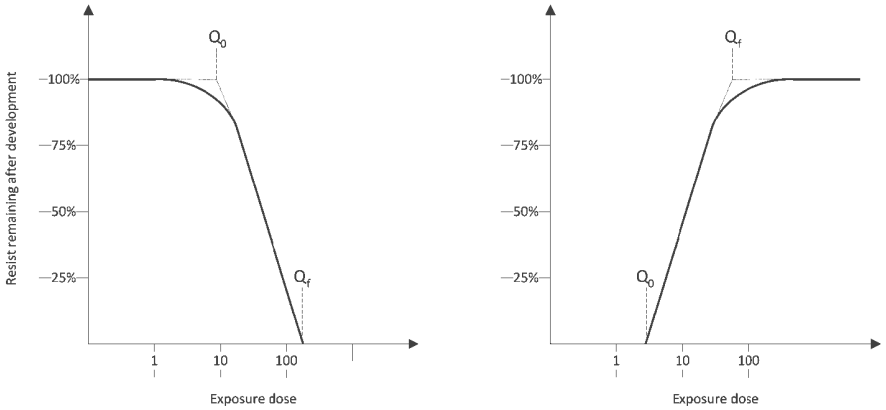

Figure 17: Resist contrast curves, an example.

metal in certain sections. There are two main parameters used to characterize photoresist: contrast and Critical Modulation Transfer Function (CMTF). Modulation transfer function is simply a measure of dark versus light intensity produced by an exposure system. CMTF is used to define the same quantity for the resist and is roughly the minimum optical transfer function needed to resolve a pattern in the resist. Contrast is an experimentally determined parameter for each resist, and its value is extracted from plots like that shown in figure 17. [9]

These plots are obtained by using different exposure doses, developing the resist and measuring the thickness that remains. For positive resist, which is shown on the left, less exposure leaves more resist. For negative resist, on the right, the opposite is true: higher exposure levels leave more resist. Contrast is the slope of the transition region in such contrast curves. Mathematically, it is defined as:

$$\gamma = \frac{1}{\log_{10} \frac{Q_f}{Q_0}} \tag{3.1}$$

where Q_0 is the exposure dose that starts the transition and Q_f is where it stops. Photolithography is the main limitation in micro-fabrication. There are several different forms of photolithography as each one progressively decrease the wavelength of light used because the highest resolution that can be achieved with photolithography is $\frac{\lambda}{4}$, in which the λ is the wavelength of the light used. UV light is the source for the vast majority of photolithography, but it has considerable drawbacks when narrowing down the length scale because it is not possible to reduce the size of the features below the diffraction limit of the UV light. Deep ultra-violet (DUV) decreases the wavelength further. Extreme UV can get a resolution of around 11 to 14 nm. [10]

There are many improvements, such as phase shift masks, Optical Proximity Correction (OPC) and high refractive index imaging. Phase shift masks use destructive interference to minimize diffraction effects. Parts of the masks that interfere with each other have a material added that would give a 90-degree phase shift to the incoming light. Then when the light meets, they will cancel and produce an area without light that was not supposed to have light before. [9] Diffraction causes the lines to be softer as they reach the surface, so edges become rounded. OPC estimates the error caused by diffraction and corrects for it by modifying the pattern structure. Diffraction effects are lessened in immersion lithography by performing lithography in a high refractive index material ($n = 1.7$). Both Intel and IBM implement immersion lithography in order to reach smaller resolution. Intel has already pushed the technology to producing 22 nm

dimensions. All of these corrections and adaptations make the photolithography system more complex and therefore more expensive.

The LIGA (Lithography, Electroplating, and Molding) process is another approach to fabricate advanced 3D structures. In this process, synchrotron generated radiation (X-ray) is used to pattern the photo resist. The process is capable of creating high aspect ratio structures (30 nm x 5 μm), but access to synchrotron radiation prohibits the usage of the method.

Multi-photon Absorption Polymerization (MAP) is another advanced technique which is used to create sophisticated 3D structures. The process utilizes a non-linear optical effect created using an ultra fast Titanium Sapphire laser. In this process, the resist is exposed to the laser and, by changing the focusing point inside the polymer; polymerization can be done according to the desired pattern. After developing the resist, un-polymerized areas can be washed away. Laser excitation can generate features with transverse dimension as small as 80 nm^2. Among these, few are highly appropriate for high resolution.

Even without the limits of resolution, photolithography is not the best candidate for advanced 3D micro-fabrication. Direct write methods allow you to create structures without the use of masks, which can decrease cost and increase the complexity (layers) in the structures. They also allow for exposure of non-planar substrates. [10] In Scanning Probe Lithography (SPL), scanning probe microscopes (SPMs) have been used to draw lines and construct nano-scale features. [11] SPL methods include Dip Pen Lithography (DPL) and Nano-imprint Lithography (NIL). DPL, which is able to pattern in the sub-100-nm scale, involves depositing an ink chemical depending on the application to the substrate via the probe. NIL mechanically

imprints patterns and demonstrated a 25-nm resolution by displacing atoms from the substrate surface.

Heated tips have shown sufficient energy to break chemical bonds of a material and decompose it into volatile monomer units, but this process was slow. Most recently, heated scanning probes have been used to write in resist. Using Self-Amplified De-polymerization (SAD) polymers, structures were written at less than 2 μs per pixel and resulted in a total write time of 143 s for an image comprising $5 * 10^5$ pixels. The tip was heated to 700 C and could create 40 nm lateral and 1 nm vertical resolution. In another study using a similar technique, resolution down to 15 nm and a writing rate of $5 * 10^4 \mu m^2$/hour was achieved. These SPL methods can be massively parallelized. Around the world, there are attempts to develop integrations of hundreds and even thousands of tips. Future densities could increase to the millions. Each tip can be either active (lowered and drawing) or passive (raised and inactive). As the head scans the substrate, basic algorithms control the tips mode in order to write the pattern. There have been several improvements to the writing speeds of these devices. [11] Although a writing time on the order of hundreds of seconds is attractive, electron beam lithography has the best advantage in resolution.

3.2 Electron Beam Litography

Another state of the art fabrication technology capable of producing high resolution patterns is Electron Beam Lithography (EBL). In EBL an electron beam is used to directly write on the surface of a sample, so it is a direct write method and does not involve masks. In the regular EBL patterning process, an electron beam is scanned across the surface exposing the

resist to enough energy to break the polymer chains throughout the entire thickness of the resist down to the substrate. Even though photolithography has been pushed by enhancements such as liquid immersion, phase-shift masks and optical proximity correction, the next-generation lithography technique of EBL offers better resolution. Early on, it was common to convert electron microscopes to EBL using accessories, but dedicated systems have produced resolutions of less than 10 nm. An EBL system is rather complex. figure 18 diagrams an EBL system based on the one used in this project. Each component will be developed in the following sub sections.

3.2.1 Electron Theory

Electrons can either act as a wave or as a particle. This wave-particle duality is routinely encountered in SEM and EBL. In both the photoelectric effect and scattering (explained more later), electrons behave like particles, but electrons are still affected by diffraction, which is a wave phenomenon. In general, electrons have lower wavelength than UV, deep UV and even Extreme Ultra-Violet (XUV) light. The wavelength of an electron is calculated by the de Broglie equation Equation 3.3.

$$\lambda = \frac{h}{p} \tag{3.2}$$

Plancks constant (h) is $6.626 * 10^{-34} \frac{kgm^2}{s}$, and p is the momentum of the electron. The momentum of an electron can be related to electron volts (eV), which is the amount of energy

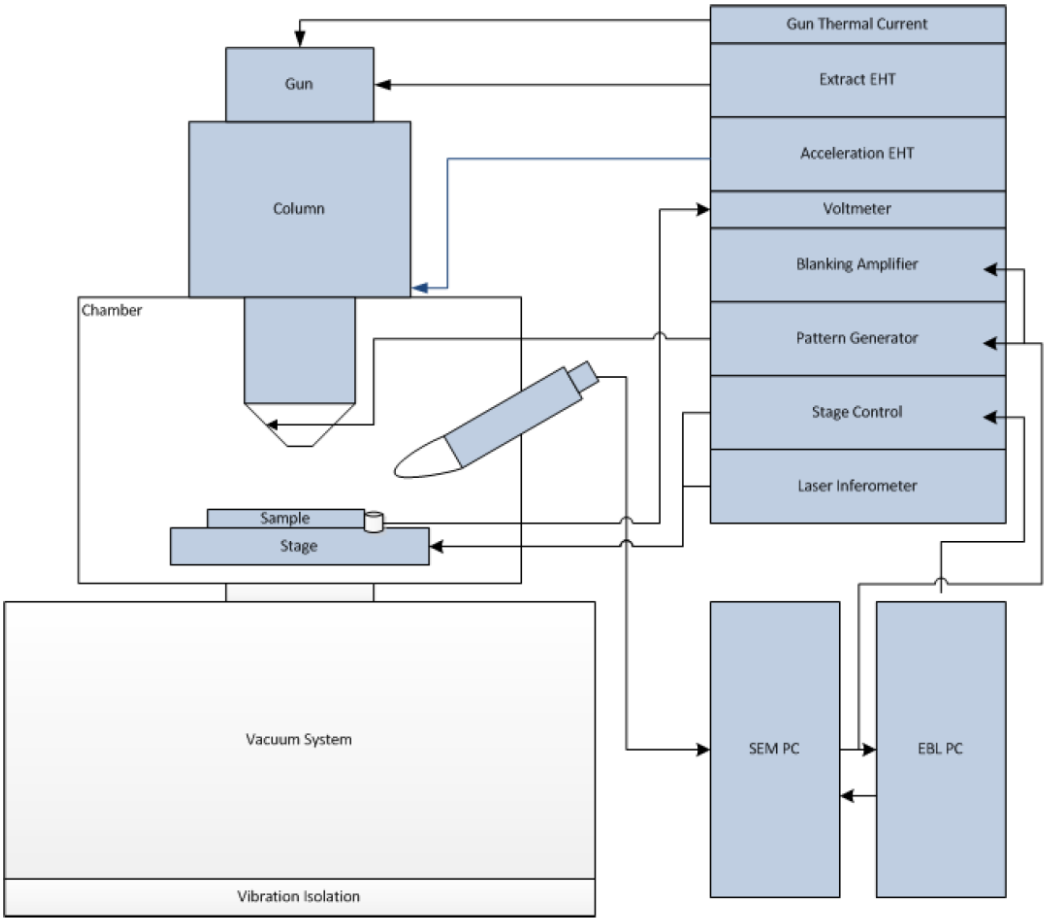

Figure 18: Schematic of an EBL system.

that an electron gains in the presence of an electric field of 1 V. For example, electrons in an SEM could be accelerated by 10 kV.

$$p = \frac{\epsilon * e}{c} = \frac{10^3 V * 1.602 * 10^{-19} C}{2.9979 * 10^8 \frac{m}{s}} = 5.344 * 10^{-24} kg \frac{m}{s} \rightarrow 0.124 nm \tag{3.3}$$

With such a low wavelength, much lower than even XUV (124 nm), the theoretical resolution is much better.

3.2.2 Vacuum Systems

One of the reasons EBL is more expensive than other lithography methods is that it requires the use of vacuum systems. A practical electron gun must operate in a vacuum. An electron is a small particle with a mass of $9.109 * 10^{-31}$ kg and can be throw off course very easily if the electron were to encounter, for example, an oxygen molecule of mass of $5.3 * 10^{-26}$ kg. There are also plenty of electron clouds of each air molecule that would deflect electrons. At atmospheric pressure (760 Torr), there are about 2.4811 * 1025 molecules in one cubic meter. In a typical vacuum of a chamber for EBL with a pressure of $1 * 10^{-5}$ Torr, there are 3.260 * 1017 molecules. This is a difference of 8 orders of magnitude, and it makes a significant difference. It is easier to see and more fitting to put it in terms of mean free path (l):

$$l = \frac{RT}{\sqrt{2}\pi d^2 N_A P} \tag{3.4}$$

where R is the universal gas constant, T is the temperature, d is the gaseous molecule's diameter, N_A is Avogadros number, and P is the pressure. Estimation is done assuming a pure nitrogen (N_2) environment, yet normal air contains 78%. This estimation also assumes the electron to be the same size as every other gas molecule. At atmosphere, the mean path is only around 0.1 nm (10^{-7} m). At the high vacuum level (10^{-5}), it is estimated around 7 m. [12] This difference is substantial, and allows for the vast majority of electrons to make it through

the electron gun unobstructed. Vacuum in the electron gun itself may be under 10^{-7} further increasing the benefits.

Vacuum plays another role. Due to the high potentials used in the electron gun, there needs to be an insulating medium (vacuum) to prevent arcing. The electrical breakdown of air is about $\frac{kV}{mm}$. [13] In high vacuum, it can be raised 10 times to 30 $\frac{kV}{mm}$. [14] This is more important in higher power (potential) equipment.

With vacuum chambers and systems, comes bake-out. This is a maintenance step where the chamber is put under vacuum and heated. The walls of the chamber heat to help vaporize materials and release gases that remain in the system. For this bake-out procedure to work, all equipment inside the chamber needs to be compatible with the temperatures used in the process. For the levels and range required, multiple stage vacuum systems are necessary. Multiple stages are used because of the different efficiencies of specific vacuum pumps. This is often the case with other fabrication equipment that require vacuum chambers such as e-beam deposition, Reactive Ion Etching (RIE) and Chemical Vapor Deposition (CVD) tools. For example, roughing pumps, which are usually piston type, are used to pump down to 10^{-3} Torr, and pumps such as turbo-molecular ones are used to pump down to higher vacuum: 10^{-5} to 10^{-7}.

3.2.3 Electron Sources

The electron gun in an EBL or SEM system needs to have a source of electrons. Electron emission involves giving enough energy to an electron so that it can overcome the binding potential (work function) and escape from the surface of a material. An example of an energy band diagram for a material, such as a metal, is represented in figure 19. The area below EV

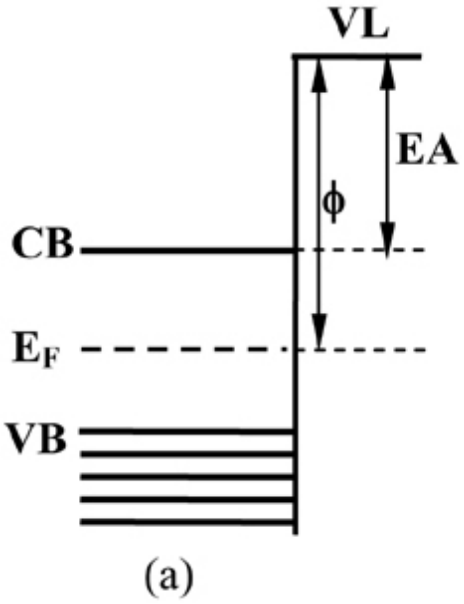

Figure 19: An example of electron band diagram.

is the valence band, where most of the electrons are in a material. The conduction band at energy Ec is the place electrons conduct in a material. The Fermi energy level, E_f, is the level at which 50% of the electrons will be found. The vacuum level, or free energy state, is that above E_0. At this energy level, the electron is no longer bound by the material. The work function ϕ is the energy needed to reach that level. Electron sources must provide a simple and consistent source of these electrons. These can be either thermionic or field emission sources.

Thermionic emission involves introducing enough energy to electrons through heat. Electrons have an energy related to temperature by the Boltzmann constant ($k = 8.617398 * 10^{-5} \frac{eV}{K}$).

$$E = kT \tag{3.5}$$

Temperature (T) is in Kelvin (K). For example, at 2700 K, electrons will have energies of about 0.23 eV. [15]

Early on, a thermionic source would simply be a thin (0.1 mm) wire of Tungsten (W). Tungsten can operate at very high temperatures without melting or evaporating. Current is run through the wire and it heats up much like a filament in a light bulb. Running this process in a vacuum helps in multiple ways. It allows the element to heat up with less energy because there are fewer molecules to allow for heat dissipation, and less air molecules prevent the filament from oxidizing. This is also why a light bulb is a vacuum. Thermionic sources are quite simple in construction and are used on various equipment such as electron beam evaporation systems. The amount of electrons emitted from a thermionic source (emission flux) can be expressed by the Richardson-Dushman equation Equation 3.6:

$$J = AT^2 \exp^{\frac{\phi}{kT}} \tag{3.6}$$

where A is a material and J is the current density emitted. For Tungsten, A equals 60 $\frac{A}{cm^2K^2}$ and the work function ϕ is 4.5 eV. From this equation, theory shows that electron current will increase exponentially with temperature. For Tungsten, this relationship is true from 2500 K to when it melts at 3100 K. Current is increased until the emission of electrons saturates. Higher

temperatures do provide more electrons, but they also sacrifice filament lifetime. At 3 to 4 A, Tungsten runs at 2500 to 2700 K. [15]

The size of emission is important because it has an effect on the overall beam size. Finer focused emission needs less area for condensing lenses, maintains a higher current density, and ultimately requires less demagnification by the column. Narrower light will also result in less energy spread, which is comparable to monochromatic light. Because of this size requirement, the shape of the source is important. Newer thermionic sources use a crystal of lanthanum hexaboride (LaB_6). The tip shape then directs emission to a narrow column. The material, also known as only lanthanum boride (LaB), is a ceramic material that has a very low work function that allows it to have some of the highest electron emissivity known.

A Wehnelt cup helps collect electrons that are emitted from the electron source. The cup encompasses the source. It is kept at a negative potential around -300 V in order to confine electrons. A small hole at the bottom of the cup allows for the electrons to be pulled toward the anode part of the electron gun.

Field Emission (FE) sources involve using an electric field that is sufficiently strong to tunnel electrons through the barrier. The sources are usually tungsten tips sharpened to a needle point. Tungsten can also be shaped to very sharp points possibly the tip of a single atom. The sharp point allows for a higher field to be active increasing electron emission and allows for tighter control of the emission location. The cathode of the source, comparative to the Wehnelt cup, is referred to as the suppressor. The anode is simply the extractor.

TABLE I: COMPARISON BETWEEN VARIOUS ELECTRON SOURCES.

Type	Brightness($\frac{Acm^2}{sr}$)	Size (nm)	Energy Spread (eV)	Vacuum required (Torr)
Thermionic: W	$\sim 10^5$	2500	2-3	10^{-5}
Thermionic: LaB_6	$\sim 10^6$	1000	2-3	10^{-6}
TFE	$\sim 10^8$	20	0.9	10^{-8}
FE	$\sim 10^9$	5	0.22	10^{-9}

Cold (field) emission sources only use the voltage as an extraction force. These sources are used primarily in electron microscopes rather than EBL because of their instability including long term drift. Newer equipment uses Mueller-emitter-based sources that are a combination of both types and known as Thermal Field Emission (TFE). These operate at high temperature and employ an extraction voltage. Heated sources are more stable because they drive off gases that might interfere with a cold source and can be stable for months at a time. Often TFE sources are tungsten tips coated with zirconium dioxide, which lowers the work function of the material. [16]

There are other electron sources being researched, such as carbon nano-tubes (CNTs). These sources offer the possibility of thermionic and photoemission. For thermionic emission, single and multi-walled CNTs intercalated with potassium, a temperature-independent work function below 600 K with a minimum of 2.0 eV has been observed. Also, Nd:YAG laser can be used to illuminate the same CNTs causing an increase in electron energy distribution. [17]

High brightness has been found in multi-walled CNTs [18], and they may prove to be a future replacement for electron sources.

3.2.4 Acceleration potential

Once you have electrons emanating from the source, they need to be accelerated down the column towards the substrate. This is done by extra-high tension through the electron gun: the source is the cathode, and at the end is the aperture, which is the anode. This EHT can range from 0 to 100 kV in EBL and even 200 kV in tunnelling electron microscopes (TEM). Higher energy electrons allow for examination of thicker sample, but they might also cause damage to the sample. Not only does higher energy pierce deep into the resist and substrate, the beam diameter also decreases. The EHT should not only be high voltage, but it must also be stable. Any change in the acceleration potential would change the energy with which the electron hits the substrate.

3.2.5 Beam blanker

In lithography, the pattern being written is not always made up of continuous lines. In order to do this, the beam will need to be stopped and started. Both the electron source and the acceleration voltage cannot be cycled off quickly. Instead, it is easier to turn the beam off and on by deflecting it from the substrate. This can be accomplished by a simple electrostatic deflector, which is a pair of plates. A blanking amplifier with fast response time is connected to the plates. When the plates are energized, the beam is deflected off its perpendicular path down the column. If the blanker is not positioned close to a focal point of the beam, streaks can occur on the sample when the beam is deflected off axis. Higher energy systems might require

elaborate blanking systems with multiple plates and delay lines in order to prevent motion of the beam during the blanking process. [16]

3.2.6 Lenses

The Wehnelt cup and the acceleration potential confine the beam a small amount and provide a coarse amount of focusing. However, the stream of electron emission is still quite divergent and requires further focusing by lenses. The goal of the lenses is to condense the electron emission into a relatively parallel (collimated) beam. In principle, lenses in electron columns behave the same as lenses in optical systems. To understand lenses in an electron column, electron trajectories can be considered like light rays, and the ideas of converging and focal points are the same.

Though electron lenses might be similar to optical lenses, the quality of the focusing in terms of aberrations is not nearly as good as with optical lenses. Spherical and chromatic aberrations are two types that are critical to EBL. Spherical aberrations are caused by a difference in power between the inner and outer areas of the lens. Chromatic aberrations occur because electrons of different energies (wavelengths/color) are focused to different points. There is no current mechanism to correct for chromatic aberrations, so narrow dispersions of the electron beam from the source are needed. Both of these aberrations can be minimized by confining the electrons to the center of the lenses, but this will greatly reduce beam current by limiting electrons.

Lenses in electron columns can either use electrostatic or magnetic forces. Electrostatic lenses are not used for fine focusing because of more serious aberrations than magnetic ones.

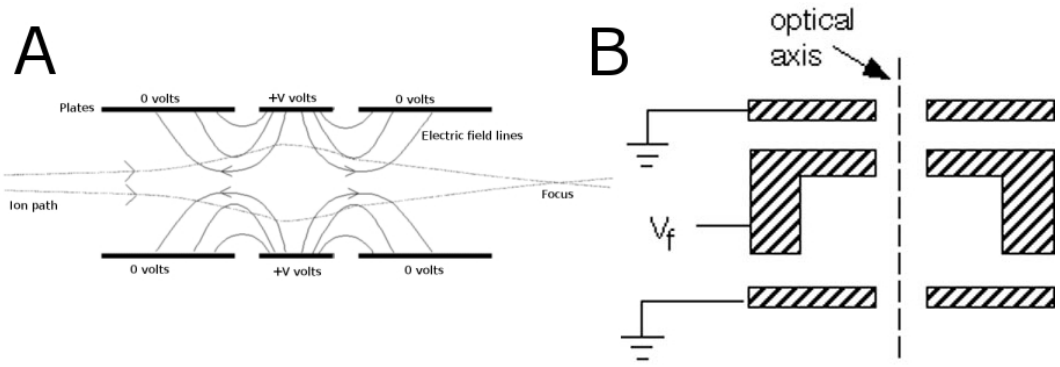

Figure 20: Einzel electrostatic lens: (A) Principle (B) Schematic.

When they are used, they are often found at the beginning of the gun region because they can be combined with the extractor anode. A simple electrostatic lens is diagramed in Figure 23.

In the Einzel lens, there are 3 apertures in series. The outer two have no potential (grounded), and the inner one has a voltage that can be varied. The focusing comes from drawing electrons back to the center of the column with positive potential. Lens power is controlled by changing the voltage. A magnetic field can be used to bend electrons inward and converge them to a focal point. This force is represented by the law of magnetic (Lorentz) force:

$$F = q\vec{v} \times \vec{B} \tag{3.7}$$

where q is the charge of an electron, $\vec{v}$ is the velocity vector of the electron and $\vec{B}$ is the magnetic field from the lens. The power of a magnetic lens can be created by using

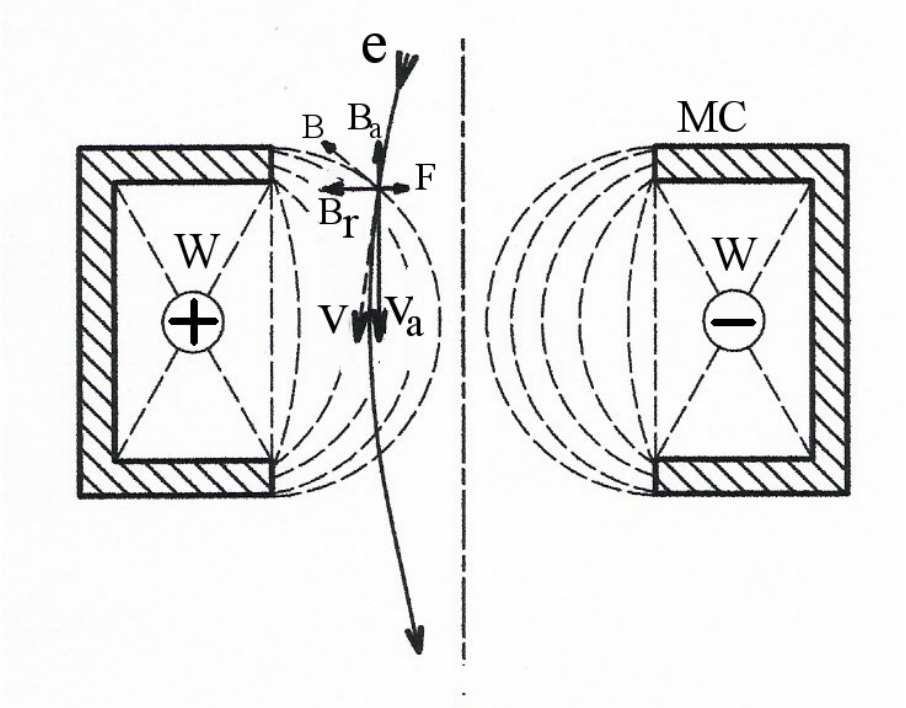

Figure 21: Cross-section of an electro-magnetic lens.

electromagnets. Electromagnets are coils of wire, usually copper, encased in a high permeability material, such as iron, to concentrate the magnetic field. An opening in the casing focuses the field toward the centre of the column.

Multiple lenses may be used to further increase the focus of the beam. The job of first condenser lens is to collect the electrons from the source. The second lens' job is to converge the beam at the specimen. The sharper the focus the fewer electrons are intercepted by the

apertures and the higher the beam current. In figure 21 it is shown a schematic of an electromagnetic lens.

3.2.7 Stigmators

Because the construction and operation of the lenses are not perfect, there will be errors in the circular beam shape. Astigmatism is an elliptical distortion of the beam caused by differences around the circumference of the lenses. Stigmators are special lenses that are used to compensate for these imperfections by adjusting X and Y directions independently. Like lenses, stigmators can be either electrostatic or magnetic. They may have 4 or more poles (8 is typical) arranged around the optical axis. There may be even two stigmators to make the beam its optimum shape.

3.2.8 Apertures

The main job of the aperture is to filter out electrons that were not tightly focused into the beam. This makes sure that the electrons are normally incident to the sample. It also intercepts the beam when it is deflected (turned off). The aperture is also used to shape the beam. Earlier beams were Gaussian in shape, but to create continuous patterns, it is useful to force the beam into a shape such as a square. Creating an area of known exposure dose makes patterning more continuous. They can then be treated as pixels and exposed individually to create patterns. Overall, different sized apertures vary the beam current.

3.2.9 Beam Scanning

Once the beam is formed, it needs to be scanned across the surface of the sample in order to render an image in an SEM or write an image in an EBL. This is done by deflecting the beam to

different parts of the sample. One scanner (deflector) tilts the beam towards another part of the sample. Alone, this would introduce an angle between the beam and the sample. Translating is done with 2 deflectors: one to tilt it to a new position, and the second to correct it back to being perpendicular to the sample. Deflecting the beam causes aberrations and enlarges the beam diameter. The maximum extent of the deflectors creates the area known as the write-field. Like lenses, beam deflectors can be either electrostatic plates or magnetic coils. Again, electromagnetic coils provide fewer distortions than the electrostatic ones; however electrostatic deflection can perform at much higher speeds. Electromagnetic coils cannot respond to the higher frequencies of charging and discharging. A compromise with both electrostatic and magnetic is used in some systems: magnetic is used for long-range deflection and electrostatic is used for short-range and high-speed. Deflection systems are frequently placed inside the final lens, so ferrite is used to cover the final lens to minimize field interactions from the scanners.

3.2.10 Stitching

Beam translation only allows for a certain write-field size that is determined by the ability of deflection and the acceptance of aberrations and distortion. In order to write patterns larger than the write-field, the sample and therefore the stage must be moved. When this process is used to continue a pattern, it is called stitching. Stage movement is done through two different methods. Coarse movement is done by servomechanisms (servos) while fine movement is done by piezoelectric motors (piezo-motors).

Servos are electric motors that involve error-feedback via encoders to allow for precise position control. Due to the mechanical nature of the servos, alone they are not accurate enough

for moving the stage. Piezo-motors rely on the change in shape of materials when voltage is applied. The deformation of these piezoelectric materials is known very precisely and allows for very fine movements. Confirmation of the movement is done on both axis (X and Y) by an interferometer. An interferometer involves using a laser to measure the distance travelled in both directions. Laser interferometers are highly accurate and allow for stitching errors to be in the range of single nanometres.

3.2.11 Substrates

There may be some limitation on what substrates are compatible with EBL. Electrons, being charged particles, tend to charge substrates negatively unless they can quickly gain a path to ground. If they are not dissipated quickly enough or become trapped, the substrate becomes charged. When a substrate is charged, it will deflect further electrons due to the repelling of similar charge. This is known as charging effect and will disrupt further exposure of the substrate. The charging effect creates the same limitation in SEM imaging that requires non-conductive samples to be coated with metal.

Especially in high-energy electron beam lithography, it is important to have paths assisting the electrons to ground. On Si wafers virtually all electrons stop at the wafer where they can follow a path to ground; however, masks, which are made of materials such as quartz (insulators), often have embedded electrons that will take much longer to move to ground. For low energy exposures, negative charge can be controlled by adding a conductive layer to insulating surfaces. For high energy exposures (¿ 10 keV), electrons can pass through the resist and conductive compensation layers and end up in the substrate.

3.2.12 Resists

SU-8 is a chemically amplified epoxy based negative UV-resist originally developed by IBM. It has shown continued use in lithography from UV in photolithography to X-ray lithography before being used in electron beam lithography. It has been extensively used in MEMS fabrication, due to its capability for high-aspect ratio structures stemming from a low absorption coefficient for wavelengths higher than 360 nm.

As already mentioned before, SU-8 is chemically amplified, meaning that exposure creates an acid that initiates cross-linking. The post-exposure bake is very critical and provides the thermal energy needed to complete the polymerization of SU-8 monomers. Overall, SU-8 seems to be the most popular resists used in several articles, such as [19]. SU-8 is developed in a PGMEA (Propylene Glycol Methyl Ether Acetate) bath. [20] It is also durable and resistant to most chemicals and solvents, which can be beneficial in processing.

PMMA is plastic that can act as a negative photoresist for EBL. Although it requires a larger exposure ($50 - 500 \frac{\mu C}{cm^2}$) dose than SU-8 ($3\ \frac{\mu C}{cm^2}$) [21], PMMA has a higher resolution [22]. It is a transparent resist that lends itself to being used for optical devices. It is also easy to apply and develop. PMMA avoids charging during EBL and exposes well. PMMA has demonstrated a 20 nm resolution [23] while another popular resist, ZEP-520, has only demonstrated 60 nm [24]. If PMMA is used on insulating substrates, a thin coating of metal, such as aluminum, chrome or copper may be used to help dissipate the charge accumulation. [25]

Chalcogenide glass (ChG) can be used by multiple sources: UV, x-ray, and e-beam. It is claimed that ChG offers many benefits over polymer resists, especially for optical device

fabrication because it is transparent in the visible and IR regions of light. This would prove important to the device in this paper. For EBL, ChG exhibits near linear height dependence with electron irradiation dose. This makes it clearer to create images from an actual structure: no correction is needed. Additional simplicity comes with the elimination of pre- and post-bake procedures that are required by polymer-based PR.

There are also several other benefits that ChG exhibits that aren't directly beneficial to this project. ChG has a much greater hardness resulting in greater etch selectivity than organic photoresists. This hardness also extended to acids, where it shows an etching ratio of around 10 via RIE, which is a five-fold increase from traditional PR. ChG allows for increased flexibility in that it acts as both a positive and negative PR depending on the alkaline developer used. Negative etch can also be performed in plasma containing CF4, Ar, and O2. The smallest features demonstrated in As35S65 ChG resist are lines of $\sim$ 17 nm width and $\sim$ 80 nm height with $\sim$ 7 nm spacing. Exposed 365-nm, 8.4 $\frac{mW}{cm^2}$, Karl SUSS MA-6 mask aligner. Etched in non-aqueous amine-based solvent. Some complications do balance out the ease that comes with ChG. As_2S_3 ChG needs to be deposited via high-vacuum thermal evaporation-deposition instead of spinning. Also, during exposure, 20 Pa of nitrogen gas (N_2) was needed to avoid charging of the substrate.

Hydrogen silsequioxane (HSQ) has been show to be an excellent tone resist in high resolution high aspect ratio EBL. It was demonstrated in multiple-step 100 keV EBL that lateral dimensions down to 30 nm in thickness up to 1 μm was possible. In these experiments, silicon nitride (Si_3N_4) was used because of the optical characteristics for x-ray lenses to reduce photon

beam absorption. Also, it allowed for the high energy EBL by sparing proximity correction. There is negligible backscattering in the thin nitride membrane. 600 K PMMA was used on top. The spot size was estimated at 10 nm with a current of 40 nA and resulted in a dose of 1000 $\frac{\mu C}{cm^2}$. Development was done in 7:3 IPA:H_2O. Samples were supercritically dried. A second layer, this time of HSQ, was applied at 1000 rpm for 60 s. 1 μm thick layer.

CHAPTER 4

CONCLUSIONS

EBL was shown to successfully write 3D patterns, which would be impossible with other binary lithography techniques. Even if it was possible, there would be alignment problems between the process steps. Grayscale lithography eliminates this by writing multiple layers in on step. When the final full-scale mold is created, it will undergo a final LIGA process. The PMMA mold will be covered in gold. This then becomes the mold for X-ray lithography, where depths of nm can be translated to cm. Here is where the true mold is produced. PDMS will then be formed by the final mold.

4.1 Analysis

In this project, a micrometer and nanometer scaled mock-up of a 3D lens mold and structure was made. Lateral dimensions met design specs, and depth was maximized in the resist. The PDMS structures were not of the quality desired. The micrometer scaled version can be considered a success even though there are plenty of improvements that can be done. The nano-scale lens will need quite a bit of enhancement in order to be considered a success for this project. Although the project was not a complete success, the proof of concept has not been disproven, and the overall concept still has promise.

4.2 Improvements

There are plenty of improvements that can be done for this project. First and foremost is the complete understanding and determination of the 3D contrast of the resist. Contrast curves were determined for different dosing of the resist, but there is still more to explore, such as maximizing depth/dose control.

- Over what area can a minimum amount of depth be written?
- Are there modifications to the PMMA that can increase the depth control?
- Can and should the process be divided into multiple layers of resist and exposure?

Even without mastering exposure, changes in the design can still lead to improvement. It was learned that at certain scales image conversion results in an over complicated pattern that can lead to excessive write times. Enlarging the pattern from the image will result in pixilation because of its bitmap nature, but what extent is this an acceptable quality sacrifice for the lens?

Acceleration potential is another value that can be adjusted. The default value of 10kV is suggested by many texts including the Raith guide. In theory, higher potential gives sharper beam size but increases back scattering. The Raith has a range of 0.2 to 30 kV, so it would help to get a characterization of how the system handles increasing acceleration potential (AP). There are few questions to be answered in testing acceleration potential:

- What is the best AP for the pattern?
- Does increased AP make higher resolution patterns?

- Does increased current speed up writing time?
- Does backscattering cause problems with the pattern?
- Is there any damage to the resist?

The aperture of 30 μm is suggested for general patterns. Larger apertures let more of the beam through: increasing beam size and overall beam current. Increased current will lower dwell time requirements. There are several questions that need to be answered:

- Does increasing beam current speed up writing time?
- Does beam diameter increase cause lower resolution?

As was stated before, the electron beam can be electromagnetically steered through different sized apertures (up to 6 on the Raith), theoretically it is possible to automatically change aperture during the writing of a pattern in order to balance speed and precision for different areas. A combination of processes could then be used. With thermal reflow, it may be possible to approximate only parts of the image and then speed up exposure. Then the image can be softened by reflow.

Working distance affects the depth of field due to the angle of approach on the sample. Farther working distance should give a cleaner and deeper exposure. This may be applicable to lines, dots and spaces, but other questions about how it affects image quality of the pattern need to be answered.

Magnification, or write-field, can also be adjusted on the EBL. Smaller write-fields should allow for more control and detail and control.

- How does magnification of the write field affect the beam deflection performance?
- Are 1000 m write fields quicker for larger patterns?
- Is the resolution of the pattern affected?

The soft-lithography portion of this project is also full of areas needing further research and improvement. Although the larger channels can easily be transferred to PDMS, the smaller (nano-scale) channels had issues. Design/shape, adhesion preventers and curing times could all have affect on the success of the smaller features. Also, when the lens is produced, the flexibility will also need to be controlled, possibly by mixture ratio or curing times or temperature.

4.3 Limitations

There are several ultimate limitations to the improvements in methods and design.One of the improvements to the design is in the use of vector format in the GDS file entirely. Limitation is imposed by the layout software. It is quite difficult to draw the complicated 3D shapes using the poly functions the software has available. For example, automating the increase in dose and size of various portions at the same time cannot be done, so most of it is manual. There is the ability to write macros for the software, but the exact use was not determined. Also, with some of the larger patterns in the layout software, errors such as too many polys and cannot fracture are encountered. Therefore, a different layout is necessary or the design needs to drawn specifically in a way that is compatible with the software. However, the time on this thesis cannot focus on all of the software aspects necessary.

The biggest down fall to electron beam lithography is long process time. Typical beam current is on the order of 10^{-9} (nA). Assuming the necessity of 10-3 $\frac{C}{cm_2}$ for exposure over a 1 cm_2 area, the resulting write time would be around 106 seconds or about 12 days.

This, ultimately, is the speed limitation of EBL. It is proven that the patterns can be done through these methods; the scaling just needs to be increased. The time of 4 - 7 days to produce a full scale model sounds absurd compared to the speed of regular photolithography, but it is not totally unacceptable. The patterning is only done to create masks. These masks are used in x-ray lithography to reproduce the true 3D mold structure. The real production is in the soft lithography process. As soon as various sized molds are produced, the production of lenses can be sped up considerably. Therefore, the speed of the EBL, at present, does not make this process infeasible.

However, the process would be greatly improved if speed was increased. This is one of the many reasons EBL is not used in mass production, such as microprocessors. One way to improve speed in EBL is using multi-beams. The company Multibeam has a technology called Complementary EBL (CEBL) in which arrays of e-beam columns are constructed in modules. Electrostatic lens are used to reduce the footprint of each column. This allows them to have 2-D arrays of 100 columns to expose 300 mm wafers, and they claim to be able to process 5 to 10 entire wafers per hour (WPH).In clustering tools, which have multiple modules, they can reach 50 to 100 WPH. There are other parallel EBL systems, such as from MAPPER Lithography. These systems use MAPPER technology with over 10,000 parallel electron beams are used to write on the surface. These systems are not just in the research phase, but they are currently

being sold. Taiwan Semiconductor Manufacturing Co. Ltd. is set to receive the Matrix 13,000 from MAPPER. Though, these systems are most likely designed for binary patterning of repeat patterns. It would be interesting to see if 3D patterning is implemented on systems like these and how much of a speed increase they offer. Advancements such as the MAPPER products make EBL technology even more attractive to use in mass nano-fabrication.

4.4 Future Research

The inability of this project to produce a full scale model lens for testing is not a reason to dismiss the entire idea; this work should continue. Several improvements, mentioned previously, should be taken into account when continuing the research. Once a more efficient design is finalized, a full scale mold should be written and a lens should be molded completely. The real determination of feasibility will come in the optical testing of an actual device. Only then will we know what improvements to make the process on a mass production scale.

APPENDIX

MATLAB CODE

A.0.1 Focalpower.m

clear all; clc; close all;

%CONSTANTS AND PRELIMINARY CALCULATIONS%

%sizes are expressed as meters%

stepsize = 250e-9;

R1 = 0.005; R2 = -0.0053; t = 0.0079; %HUGHES nlens = 1.4532; %refractive index of rabbit eye naq = 1.3346; %vitreous liquid refractive index

neff = (nlens - naq)/naq; %effective refractive index

%LENSMAKER'S EQUATION - GENERAL CASE%

P = (neff)*(1/R1 - 1/R2 + ((neff*t)/(nlens*R1*R2))); %focal power of the normal two-sided lens in meters f = 1/P; %focus distance

%PLANO-CONVEX LENS DESIGN%

%nlens = 1.493; %refractive index of PMMA nlens = 1.41; %refractive index of PDMS

neff = (nlens - naq)/naq;

R1pc = neff/P;

dpc = 2*R1pc; nstep = R1pc/stepsize

APPENDIX (Continued)

A.0.2 Upperlens.m

% Design of the upper lens (most external one)

function [x, y, thickness] = upperlens(radius, lensdiameter, precision)

thickness = radius - sqrt(radius$\hat{2}$ - (lensdiameter/2)$\hat{2}$); center = [0, thickness-radius];

x = linspace(-lens_diameter/2, lensdiameter/2, precision); y = sqrt(radius.$\hat{2}$ - (x-center(1)).$\hat{2}$) + center(2);

A.0.3 Lowerlens.m

function [x, y, thickness] = lower_lens(radius, lens_diameter, precision)

thickness = radius - sqrt(radius$\hat{2}$ - (lens_diameter/2)$\hat{2}$); center = [0, radius-thickness];

x = linspace(-lens_diameter/2, lens_diameter/2, precision); y = -sqrt(radius.$\hat{2}$ - (x-center(1)).$\hat{2}$) + center(2);

A.0.4 Doublesidedlens.m

% All units in um format long e; clear all; clc; close all;

% CONSTANTS N = 1e6; % Evaluation points (10$\hat{6}$ for external teeth)

substrthick = 250e-3; % Thickness of the substrate interlayer = 500; % Thickness of the spiral part

% RABBIT %

radiusupunacc = 8e3; radiuslowunacc = 7e3; lensdiameterunacc = 11e3;

% radiusupunacc = 5e3; % radiuslowunacc = 5.3e3; % lensdiameterunacc = 11e3;

% radiusupacc = 7.5e3; % radiuslowacc = 5.5e3; % lensdiameteracc = 8.5e3;

% UNACCOMODATED LENS

APPENDIX (Continued)

% Upper lens (most external one) - Unaccomodated [xupunacc, yupunacc, thicknessupunacc] = ... upperlens(radiusupunacc, lensdiameterunacc, N); % Lower lens (most internal one) - Unaccomodated [xlowunacc, ylowunacc, thicknesslowunacc] = ... lowerlens(radiuslowunacc, lensdiameterunacc, N);

% Plot of the actual lenses - Unaccomodated

subplot(2,2,1); plot(xupunacc, yupunacc); hold on; title('Unaccomodated lens'); plot(xlowunacc, ylowunacc, 'r'); xlabel('Lens diameter (mum)'); ylabel('Lens thickness (mum)'); xlim([-5e3, 5e3]);

% Correcting offset for exact thickness of the central lens

yupunacc = ... yupunacc + substrthick - rem(thicknessupunacc, substrthick); ylowunacc = ... ylowunacc - substrthick + rem(thicknesslowunacc, substrthick);

% Plot of Fresnel lenses - Unaccomodated

yupFresnelunacc = ... mod(yupunacc, substrthick) + interlayer/2; ylowFresnelunacc = ... mod(ylowunacc, substrthick) - substrthick - interlayer/2; subplot(2,2,2); plot(xupunacc, yupFresnelunacc); hold on; title('Unaccomodated Fresnel lens'); plot(xlowunacc, ylowFresnelunacc, 'r'); xlabel('Lens diameter (mum)'); ylabel('Lens thickness (mum)');

% ACCOMODATED LENS

% Upper lens (most external one) - Accomodated

[xupacc, yupacc, thicknessupacc] = ... upperlens(radiusupacc, lensdiameteracc, N); % Lower lens (most internal one) - Accomodated [xlowacc, ylowacc, thicknesslowacc] = ... lowerlens(radiuslowacc, lensdiameteracc, N);

APPENDIX (Continued)

% Plot of the actual lenses - Accomodated subplot(2,2,3); plot(xupacc, yupacc); hold on; title('Accomodated lens'); plot(xlowacc, ylowacc, 'r'); xlabel('Lens diameter (mum)'); ylabel('Lens thickness (mum)'); xlim([-5e3, 5e3]);

yupacc = ... yupacc + substrthick - rem(thicknessupacc, substrthick); ylowacc = ... ylowacc - substrthick + rem(thicknesslowacc, substrthick);

yupFresnelacc = ... mod(yupacc, substrthick) + interlayer/2; ylowFresnelacc = ... mod(ylowacc, substrthick) - substrthick - interlayer/2; subplot(2,2,4); plot(xupacc, yupFresnelacc); hold on; title('Accomodated Fresnel lens'); plot(xlowacc, ylowFresnelacc, 'r'); xlabel('Lens diameter (mum)'); ylabel('Lens thickness (mum)');

% EXTRA CENTRAL GRAPHIC PART j = 1; k = 1; for i = 1:N if (xupunacc(i) ¿ -140 AND xupunacc(i) ¡ 130) xunaccshort(j) = xupunacc(i); yupFresnelunaccshort(j) = yupFresnelunacc(i); ylowFresnelunaccshort(j) = ylowFresnelunacc(i); j = j + 1; end if (xupacc(i) ¿ -140 AND xupacc(i) ¡ 130) xaccshort(k) = xupacc(i); yupFresnelaccshort(k) = yupFresnelacc(i); ylowFresnelaccshort(k) = ylowFresnelacc(i); k = k + 1; end end

figure; subplot(2,1,1); plot(xunaccshort, yupFresnelunaccshort, 'k'); hold on; grid on; grid minor; plot(xaccshort, yupFresnelaccshort, 'r'); legend('Unaccomodated lens', 'Accomodated lens'); xlim([-130, 130]); ylim([249.9, 250.4]);

subplot(2,1,2); plot(xunaccshort, ylowFresnelunaccshort, 'k'); hold on; grid on; grid minor; plot(xaccshort, ylowFresnelaccshort, 'r'); legend('Unaccomodated lens', 'Accomodated lens'); xlim([-130, 130]); ylim([-250.4, -249.9]);

APPENDIX (Continued)

% SPIRAL CUT j = 1; k = 1; for i = 1:length(xunaccshort) if (xupunacc(i) ¿ -140 AND xupunacc(i) ¡ 130) xunaccshort(j) = xupunacc(i); yupFresnelunaccshort(j) = yupFresnelunacc(i); ylowFresnelunaccshort(j) = ylowFresnelunacc(i); j = j + 1; end if (xupacc(i) ¿ -140 AND xupacc(i) ¡ 130) xaccshort(k) = xupacc(i); yupFresnelaccshort(k) = yupFresnelacc(i); ylowFresnelaccshort(k) = ylowFresnelacc(i); k = k + 1; end end

CITED LITERATURE

1. Dubbelman, M.: "the shape of the aging human lens: curvature, equivalent refractive index and the lens paradox". Vision Research, pages 184–198, 2006.

2. Tsonis, P. A.: The rabbit in cataract/iol surgery. Animal Models in Eye Research, pages 184–198, 2008.

3. Buser, P. and Imbert, M.: Vision. MIT Press, 1992.

4. Wikipedia: http://en.wikipedia.org/wiki/optics. Retrieved 04/23/2014 from http://en.wikipedia.org/wiki/Optics.

5. Jayapratha, N.: Implantable Intraocular Lens with Changing Focal Distances. University of Illinois at Chicago: Chicago, 2011.

6. Zaker, E.: Nano-fabrication of Accommodative Intraocular Lenses Using Gray-Scale Electron Beam and Soft Litography. University of Illinois at Chicago: Chicago, 2012.

7. Mazza, F.: Implantable Human Lenses with Adjustable Focal Distance as a Solution for Cataract Treatment. University of Illinois at Chicago: Chicago, 2014.

8. Liu, C.: Foundations of MEMS. Upper Saddle River, NJ: Pearson Education, Inc. 530, 2006.

9. James, D. and Plummer, M.: Silicon VLSI Technology. Upper Saddle River, NJ: Prentice Hall, Inc., 2000.

10. Afromowitz, M.: Photolithography with a twist: A workshop on gray scale and 3-d methods.

11. Arbuckle, D. and Requicha, A.: Massively parallel scanning probe nanolithography. Nanotechnology, IEEE-NANO 2003. 2003 Third IEEE Conference on., 2003.

12. Nave, C.: Mean free path calculation. Retrieved 04/18/2014 from http://hyperphysics.phy-astr.gsu.edu/hbase/kinetic/menfre.html.

CITED LITERATURE (Continued)

13. Elert, G.: Dielectric strength of air. The Physics Factbook, 2009.

14. Giere, S., K. M. and Schumann, U.: Hv dielectric strength of shielding electrodes in vacuum circuit-breakers. Discharges and Electrical Insulation in Vacuum, 2002, 20th. International Symposium on, 2002.

15. Wittke, J.: Electron column: Electron source. glg 510 - course overview. Retrieved 04/18/2014 from http://www4.nau.edu/microanalysis/Microprobe/Column-ElectronGun.html, 2003.

16. for Nanoscale Science, C. and University., T. N.: SPIE Handbook of Microlithography, Micromachining and Microfabrication, 2010.

17. Westover, T.L., e. a.: Photo and thermionic emission from potassium-intercalated carbon nanotube arrays. Journal of Vacuum Science & Technology B: Microelectronics and Nanometer Structures, 28(2):423–434, 2002.

18. de Jonge, N., L. Y. S. K. and Oosterkamp, T.: High brightness electron beam from a multi-walled carbon nanotube. Journal of Vacuum Science & Technology B: Microelectronics and Nanometer Structures, 420:3, 2002.

19. Kuo-Shen, C., L. I. and Fu-Hsang, K.: Fabrication of 3d polymer microstructures using electron beam lithography and nanoimprinting technologies. Journal of Micromechanics and Microengineering, 15(10):1894, 2005.

20. Bilenberg, B., e. a.: High resolution 100 kv electron beam lithography in su-8. Journal of Micromechanics and Microengineering, 83(49):1609–1612, 2006.

21. Dong, L., P. S. and Friberg, A.: One-step fabrication of polymer components for microphotonics by gray scale electron beam lithography. Journal of the European Optical Society - Rapid publications, 11010(6), 2011.

22. Hung-Lin, Y., H. J. and Chih-Sheng, Y.: The study on 3d electron beam lithography for sub-micrometer diffractive optics. in optical mems and nanophotonics. 2007 IEEE/LEOS International Conference, 2007.

23. Cumming, e. a.: Fabrication of 3 nm wires using 100 kev electron beam lithography and poly(methyl methacrylate). Melville, NY, US: American Institute of Physics, 68(3), 1996.

CITED LITERATURE (Continued)

24. Ye, H., e. a.: 1st ieee intl. conf. on nano/micro engineered and molecular systems. 2006.

25. Muhammad, M., e. a.: Nanopatterning of pmma on insulating surfaces with various anticharging schemes using 30 kev electron beam lithography. Journal of Vacuum ScienceTechnology B: Microelectronics and Nanometer Structures, 29(6):06F304–6.

26. Goldstein, B.: Sensation and Perception (7th Edition). Cengage Learning, 2007.

27. Baumeister, M. and Kohnen, T.: Akkommodation und presbyopie: Teil 1: Physiologie der akkommodation und entwicklung der presbyopie. Der Ophthalmologe, 105(6):597–610, June 2008.

28. Goldberg, D. B.: Computer-animated model of accommodation and theory of reciprocal zonular action. Clinical Ophhthalmology, 5:1559–1566, 2011.

29. Mathias, R. T., White, T. W., and Gong, X.: Lens gap junctions in growth, differentiation, and homeostasis. Physiological Reviews, 90(1):179–206, January 2010.

30. Tasman, W. and Jaeger, E. A.: Duane's Ophthalmology (CD-ROM). Lippincott, Williams & Wilkins, 2006.

31. Steinert, R. F.: Cataract Surgery (3rd Edition). Elsevier Inc., 2010.

32. Dealye, M. and Tardieu, A.: Short-range order of crystallin proteins accounts for eye lens transparency. Nature, 302:415–417, March 1983.

33. Congdon, N., Vingerling, J. R., Klein, B. E., et al.: Prevalence of cataract and pseudophakia/aphakia among adults in the united states. Archives of Ophthalmology, 122(4):487–494, April 2004.

34. Baltussen, R., Sylla, M., and Mariotti, S.: Cost-effectiveness analysis of cataract surgery: a global and regional analysis. Bulletin of the World Health Organization, 82(5):338–345, May 2004.

35. Henderson, B. A., Pineda, R., Ament, C., and Chen, S. H.: Essentials of Cataract Surgery. SLACK Inc., 2007.

36. Meda, N., Bognounou, V., et al.: Cataract in burkina faso: Factors of choice between modern and traditional surgical procedures. Medecine Tropicale, 65(5):473–476, 2005.

CITED LITERATURE (Continued)

37. Prajna, N. and Chandrakanth, K.S., e. a.: The madurai intraocular lens study. ii: Clinical outcomes. American Journal of Ophthalmology, 125(1):14–25, 1998.

VITA

Name:

Mattias Mengoni

Education:

Laurea in Ingegneria Elettronica, Universitá Politecnica delle Marche, Ancona, Italy, 2011.
Laurea Magistrale in Ingegneria Elettronica (Electronic Engineering), Politecnico di Torino, Turin, Italy, 2014.
Master of Science in Electrical and Computer Engineering, University of Illinois at Chicago, Chicago, 2014.

Honours and Awards:

TOP-UIC Scholarship, Politecnico di Torino and University of Illinois at Chicago
Superbravo Award, Universitá Politecnica delle Marche and ITIS Vito Volterra
Leonardo da Vinci LLP Scholarship, High School ITIS Vito Volterra and Institut Comte de Rius